Cryogenic fluid dynamics

1999 J. Phys.: Condens. Matter 11 7783

(http://iopscience.iop.org/0953-8984/11/40/309)

J. Phys.: Condens. Matter **11** (1999) 7783–7834. Printed in the UK PII: S0953-8984(99)06550-9

Cryogenic fluid dynamics

Russell J Donnelly

Cryogenic Helium Turbulence Laboratory, Department of Physics, University of Oregon, Eugene, Oregon 97403-1274, USA

Received 2 August 1999

Abstract. The uses of liquid helium I, liquid helium II and gaseous helium near its critical point in experimental investigations are emerging as an important branch of modern fluid dynamics. This paper is an attempt to review the use of liquid helium in research on stability, transition and turbulence. Emphasis is made on the contributions of W F Vinen to turbulence studies in helium II.

1. Introduction

The purpose of the papers in this special issue of the *J. Phys.: Condens. Matter* is to bring some mature reflection to the scientific contributions of William Frank Vinen, known for reasons obscure to his colleagues as 'Joe'. The authors believe that few scientists active in the field of classical turbulence are in a position to appreciate fully the remarkable discoveries and insights which Vinen has brought to the study of turbulent flow in liquid helium II. This paper is an attempt to remedy this defect by demonstrating, through the historical record, Vinen's seminal role in the evolution of this subject, and the future we see before us.

Although this paper is in some sense a review of the subject, it has no pretense to completeness. The counterflow problem itself has elicited hundreds of papers and it would make no sense to try to discuss them all, especially since our view of the subject has changed steadily over the years. Similarly, I have drawn heavily on past review articles (often by present and past members of our group) to put together this article.

Cryogenic helium is important not only for studies of turbulence, but also for wind tunnel testing and modelling of surface ships on tow tanks. This paper is restricted to the instability and turbulence problems. Substantial accounts of these other uses of cryogenic helium are contained in the proceedings of two conferences on the subject, Donnelly (1991a) and Donnelly (1998), as well as a paper by Skrbek, Niemela and Donnelly elsewhere in this issue, based on a talk by Skrbek at Vinen's recognition meeting.

It might be useful to record here how I first met Joe Vinen. In 1955 two announcements appeared by Wheeler, Blakewood and Lane (Wheeler *et al* 1955a, b) investigating flow between concentric rotating cylinders by means of second sound attenuation. News of this experiment reached Cambridge and David Shoenberg, adviser to Joe Vinen and Henry Hall, wrote to our adviser, Cecil T Lane, noting that related experiments were going on at the Royal Society Mond Laboratory. We students soon got in touch, and when I started teaching at the University of Chicago, Henry and Joe paid a visit on a hot summer day, arriving in Hyde Park by the Illinois Central elevated train. Thus began a scientific and personal relationship which has lasted ever since.

0953-8984/99/407783+52$30.00

On that first visit to the USA, Joe and Henry visited Dick Feynman at CalTech and described their work on quantized vortices to him. Much of what both Onsager and Feynman had predicted about quantized vortices turned out to be true. As Feynman remarked to me later: 'They made it real'. A little more historical insight into this achievement is contained in section 4.2.1.

While many of us studying superfluidity recall the '*annus mirabilis*' of Hall and Vinen's work establishing the reality of quantized vortices, few have understood the significance of four papers published by Vinen in *Proceedings of the Royal Society* on the turbulent flow of helium II (Vinen 1957a, b, c, 1958). These papers were followed by a comprehensive review on all aspects of quantized vortex lines (Vinen 1961b). This paper attempts to remedy that situation.

2. Turbulence in cryogenic helium

2.1. Characteristics of various fluids available for turbulence studies

Most natural turbulent phenomena occur on large scales L and are therefore characterized by large Reynolds numbers

$$Re = \frac{UL}{\nu} \tag{2.1}$$

and Rayleigh numbers

$$Ra = \frac{g\alpha\Delta T L^3}{\nu\kappa} \tag{2.2}$$

where U is a characteristic velocity, ν denotes the kinematic viscosity, α is the thermal expansion coefficient, κ the thermal diffusivity, ΔT stands for the temperature difference and g is the acceleration due to gravity

It is only in the last ten years or so that the significance of the fact that cryogenic helium has the lowest viscosity of any known material has been appreciated. The low kinematic viscosity can be exploited to generate conventional classical turbulence at very high Reynolds numbers and Rayleigh numbers. Critical helium gas, helium I (the higher temperature phase of liquid helium) and helium II (the phase below the lambda transition, which displays superfluidity) are all useful in this respect (Donnelly 1991a, b). In fact the need for generating the highest Reynolds numbers for engineering purposes can be fully met by the use of cryogenic helium. Unlike classical fluids such as water and air, the conditions which prevail in using cryogenic fluids allow the use of both temperature and pressure as ways of varying the physical properties of the fluids. Thanks to the demand for large-scale refrigeration for superconducting magnets in high-energy and nuclear physics, the facilities to use helium in large-scale experiments are already at hand in a number of laboratories both in the United States and abroad.

A more complete discussion of the properties of helium relevant to cryogenic turbulence research is contained in the companion paper by Skrbek, Niemela and Donnelly in this issue. The authors also discuss a number of uses for cryogenic helium which are beyond the scope of the present paper. These include short descriptions of helium flow tunnels, the characteristics of liquid helium tow tanks and convection experiments in critical helium gas.

2.2. Importance of turbulence research

If one is to embark on a new program of turbulence research using cryogenic helium, then it is significant to understand why this should be done at all. Fluid turbulence is undoubtedly

the most outstanding problem of classical physics that has remained unsolved to this day. It is a paradigm for spatio-temporal systems with many degrees of freedom interacting strongly nonlinearly. The intellectual stimulus that the turbulence problem has provided for the advancement in nonlinear science and chaos, field theoretical methods, advanced instrumentation, numerical and computational schemes, and so forth, has been extraordinary. On the practical side, turbulence is the 'limiting factor' in the design and operation of various energy systems in aeronautical, chemical and mechanical engineering, as well as geophysics, meteorology and other areas which strongly impact human life. For these reasons, an enhanced ability to understand and predict turbulent flows will have a large payoff. The most eloquent remarks in this regard were made by von Neumann (1949),

'The great importance of turbulence requires no further emphasis. Turbulence undoubtedly represents a central principle for many parts of physics, and a thorough understanding of its properties must be expected to lead to advances in many fields. . . . turbulence represents *per se* an important principle in physical theory and in pure mathematics.

. . . These considerations justify the view that a considerable effort towards a detailed understanding of the mechanisms of turbulence is called for.'

These remarks are just as true today.

Turbulence is intrinsically a high-Reynolds-number phenomenon, and it has always been clear that its quantitative understanding requires, most of all, precise data at high Reynolds numbers. In thermal convection experiments the Reynolds number is roughly the square root of the Rayleigh number. Thus, very large Rayleigh numbers imply large Reynolds number as well. To quote von Neumann again:

'. . . our intuitive relationship to the subject is still too loose . . . (and) we are still disoriented as to the relevant factors . . . .'

At present, there are few opportunities for making detailed and extensive measurements at high Reynolds numbers with the required degree of control and precision. Even those aspects of turbulence which are understood qualitatively still rest on uncertain ground—at least because the theory seeks to understand infinitely large Reynolds numbers. While experiments and numerical simulations have, by and large, been carried out at low or moderate Reynolds numbers, such measurements cannot often make the needed distinction between the predictions of conflicting theories. While the high-Reynolds-number experiments in the atmosphere and oceans have contributed much to our understanding of turbulence, they suffer from the fact that experimental conditions are very hard to control, hence these flows are not ideal for settling crucial questions. Well planned experiments which combine careful experimental control and truly high Reynolds and Rayleigh numbers will provide fundamental new insights into modern theories of turbulence.

3. Turbulence in helium I

3.1. High-Reynolds-number pipe flow

Both liquid helium I and critical helium gas can be utilized in achieving classical (Newtonian), incompressible or (with the gas) compressible turbulent flows. The parameter of interest in incompressible turbulence is the flow velocity, characterized by the Reynolds number

$Re = UL/\nu$, where U is a characteristic velocity and L is a characteristic length. As we have noted, the kinematic viscosity of helium is much lower than that of water or air. For instance, for water at 20 °C and helium I at 2.18 K, $\nu_{\text{water}}/\nu_{\text{He I}} = 59$, and for $\nu_{\text{air}}/\nu_{\text{He I}} = 869$. Using helium I it should be possible to reach Reynolds numbers comparable to the best existing wind tunnels with a compact, relatively low-cost flow facility.

Although helium I does not suffer from non-classical behaviour (such as the superfluidity of helium II), the reduced scale of high-Reynolds-number experiments does have its problems. Because the size of a helium tunnel may be so much smaller than air or water tunnels, one must consider miniaturized instrumentation. Of primary concern is the small scale of the flow structures such as turbulent eddies and boundary layers. Consider flow through a smooth pipe at high Reynolds number. To be definite let us take a pipe 10 cm in diameter with liquid helium having a kinematic viscosity $\nu = 2 \times 10^{-4}$ cm^3 s^{-1} flowing at a mean velocity $\bar{u}$, and density $\rho = 0.146$ g cm^{-3}. For turbulent flow a viscous sublayer is generated at the walls which scales with the friction velocity. The friction velocity is given by $u^* = \sqrt{\tau/\rho}$, where τ, the wall stress, is $\tau = \lambda\rho u^2/8$ and λ is the empirical friction factor (Schlichting 1979). The corresponding length scale is

$$y = \frac{\nu}{u^*} \tag{3.1}$$

and the viscous sublayer has a thickness of a few times y. Thus y can be thought of as the scale of the smallest eddies in the turbulent flow. Table 1 outlines some typical values for helium I.

Table 1. Viscous sub-layer thickness at various Reynolds numbers.

$\bar{u}$ (cm s^{-1})	Re	λ	τ (erg cm^{-3})	u^* (cm s^{-1})	y (cm)
10	5×10^5	0.0132	0.0240	0.405	4.93×10^{-4}
10^2	5×10^6	0.008 98	1.64	3.35	5.97×10^{-5}
10^3	5×10^7	0.006 49	118.4	28.48	7.02×10^{-6}
10^4	5×10^8	0.004 89	8940	247	8.08×10^{-7}
2×10^4	1×10^9	0.004 53	33 100	476	4.20×10^{-7}

Note that in helium I we can in principle use velocities of flow up to the velocity of sound before encountering shock waves. We cannot use such large velocities in helium II because second sound shock waves will intrude at about an order of magnitude lower velocity. The speed of sound in the gas is lower than in the liquid, hence the highest pipe flow Reynolds numbers generated with cryogenic helium should be generated with helium I.

It can be seen that the length scales can range from micrometres to Ångstroms. For comparison with theories it is important to be able to probe the flow at the smallest scales. Probing the flow will be a major instrumentation challenge. It is necessary to learn to build micrometre or even nanometre-sized transducers to take advantage of the new range of high Reynolds numbers afforded by helium.

3.2. Bénard convection

Above about 2.2 K liquid helium is assumed to behave as an ordinary incompressible Newtonian fluid, free from the macroscopic quantum effects possessed by its lower temperature counterpart. One suitable test of this assumption is to compare the observed onset and nature of hydrodynamic instabilities in helium with detailed predictions based on the stability equations derived for ordinary incompressible fluids.

A particularly simple and experimentally accessible hydrodynamic system is Rayleigh–Bénard convection which we introduced in section 2.1. The use of helium I as a medium for studying convective flows has been recently reviewed by Behringer (1990). The critical Rayleigh numbers for the onset of convection are approximately the same in water and in helium I, furthermore the shapes of the Nusselt number–Rayleigh number curves beyond critical are also similar. Niemela and Donnelly (1991) have also exploited a special case in which the heating is periodically varied in time, a subject of current interest both theoretically and experimentally, and for which a number of novel states of the system can be investigated via tuning of the appropriate external parameters. Parametrically modulated systems are not always turbulent, and are beyond the scope of this article. Interested readers can find a review in Donnelly (1989).

In order to have a more universal measure of the state of the Rayleigh–Bénard system, the vertical temperature difference is usually made non-dimensional in terms of the Rayleigh number. In practice, the finite geometry of the experimental cell, as well as imperfect thermal boundary conditions, have some influence on the correspondence between a particular value of the Rayleigh number and the state of stress of the system, so that a more accurate representation of the latter is to use a *reduced* Rayleigh number

$$\varepsilon = R\alpha / R\alpha_c - 1 \tag{3.2}$$

where $R\alpha_c$ is the critical value of the Rayleigh number determined at the onset of convection. In addition, particular fluids may be characterized by the ratio of kinematic viscosity to thermal diffusivity, or Prandtl number

$$\sigma = \upsilon / \kappa. \tag{3.3}$$

Helium I has a Prandtl number varying with the temperature from slightly less than $\sim 1/2$ to about $3/4$, where by comparison σ is about $2/3$ for ideal gases, 6 for water and about 200 for silicone oils.

There are a number of technological advantages to using helium I as a working fluid, such as the existence of a well developed cryogenic technology for precise temperature measurement and control. Another advantage is the large ratio of thermal diffusivities of the solid (copper) horizontal boundary plates to the enclosed fluid at very low absolute temperatures. This enables fast and virtually unattenuated reception of high-frequency temperature fluctuations, an extremely useful attribute, for instance, in the study of time-periodic or turbulent convective flow. Conversely, one can also easily *apply* a time-dependent fluctuation of the temperature to the fluid. This suggests a class of experiments which was mentioned above; namely, the temporal modulation of the buoyancy force which drives the convective flow. This area of investigation was originally motivated, at least in part, by similarities to the well known problem of the inverted physical pendulum which can be made to execute stable oscillations in an *upright* position via vertical modulation of its point of support. In the hydrodynamic analogue, enhanced stability is achieved by allowing the temperature difference across a layer of fluid to possess both a steady mean value and an oscillating component such that $\Delta T(t) = \Delta T\{1 + \Delta \cos(\omega t)\}$. The reduced Rayleigh number for this problem is then defined as $\varepsilon = Ra/Ra_c^{STAT} - 1$, where Ra_c^{STAT} is the critical value of the Rayleigh number in the absence of modulation and here Ra is taken to be averaged over the modulation cycle. In this system the conducting state of the fluid for a range of mean Rayleigh numbers *greater* than Ra_c^{STAT} is made stable by this periodic modulation of the instantaneous temperature difference. That is, while standard Rayleigh–Bénard convection is initiated, by definition, at $\varepsilon_c = 0$, the convective threshold with modulation is shifted to higher values of the control parameter, $\varepsilon_c > 0$.

3.3. Drag on a sphere

One characteristic of classical turbulent flow is evidenced by the celebrated relationship between drag coefficient and Reynolds number for flow about a sphere. At a Reynolds number of about 2×10^5 there is a sudden fall in the drag coefficient which has been known for decades. The question of whether that fall exists in helium I and helium II was first taken up by Laing and Rorschach (1961) with somewhat inconclusive results. A discussion of such early measurements is contained in Donnelly (1991a). Recently, Smith *et al* (1999) have built an apparatus which establishes the drag on the sphere in both helium I and helium II by direct measurement of the pressure distribution as shown in figure 14. The results are discussed in section 4.7.4.

4. Turbulence in helium II

4.1. The two-fluid model and second sound

Helium II acts hydrodynamically as if it were a mixture of a normal fluid of density ρ_n and velocity v_n and a superfluid of density ρ_s and velocity v_s. The superfluid appears to carry no entropy, and the entire heat content of the fluid must be added to convert a mass of superfluid to normal fluid. The total density

$$\rho = \rho_n + \rho_s \tag{4.1}$$

is about 0.14 g cm^{-3}. Under modest chemical potential gradients the superfluid can flow with no measurable friction, and flow states can be set up in toroidal apparatus which appear to persist indefinitely.

The normal fluid has a viscosity of order 20 $\mu\rho$ and tends to be immobilized in porous powders of size less than about 1 μm. The superfluid, however, is not so hindered, and flows easily through the finest channels one can manufacture. Porous media, then, form a semipermeable separator for helium II, passing the superfluid and not normal fluid. A temperature difference ΔT across such a barrier will develop a 'fountain pressure' ΔP, and these variables are related to the entropy per unit mass S by

$$\frac{\Delta P}{\Delta T} = \rho S. \tag{4.2}$$

Suppose liquid helium is contained in a tube with a closed end fitted with a heater, as shown schematically in figure 2(b), and the heater supplies heat flux q (W cm^{-2}). When heat is supplied, the superfluid will flow towards the heater, pick up heat content, transform to normal fluid and flow away from the heater out to the helium bath. This peculiar counterflow has no net mass flux, i.e.

$$j = \rho_n v_n + \rho_s v_s = 0 \tag{4.3}$$

and since the superfluid has no entropy, the heat flux is $q = \rho S T v_n$. If the heat is switched on and off periodically, the two fluids will execute small-amplitude counterflow described by a standing wave of second sound. Second sound is a wave of temperature difference in helium II which has low natural attenuation and very little dispersion. Second sound is an important tool in turbulence research because it is strongly attenuated by quantized vortices.

The combined evidence of the above and other experiments leads to the two-fluid equations of motion first put forward by Tisza (1938) and Landau (1941) (for a rigorous discussion, see Roberts and Donnelly 1974)

$$\rho_s \frac{\mathrm{D}\boldsymbol{v}_s}{\mathrm{D}t} = -\frac{\rho_s}{\rho}\nabla P + \rho_s S \nabla T - \boldsymbol{F}_{ns} \tag{4.4}$$

$$\rho_n \frac{\mathrm{D}\boldsymbol{v}_n}{\mathrm{D}t} = -\frac{\rho_n}{\rho}\nabla P + \rho_s S \nabla T + \boldsymbol{F}_{ns} + \eta \nabla^2 \boldsymbol{v}_n \tag{4.5}$$

where η is the coefficient of shear viscosity and $\boldsymbol{F}_{ns}$ is a mutual friction force between the normal fluid and superfluid which we will discuss in section 4.2.2, and which is zero in the absence of quantized vortex lines (see below). To these are added conservation equations for mass and entropy

$$\frac{\partial \rho}{\partial t} + \mathrm{div}(\rho_s v_s + \rho_n v_n) = 0 \tag{4.6}$$

$$\frac{\partial}{\partial t}\rho S + \mathrm{div}(\rho S v_n) = 0 \tag{4.7}$$

and the equation for the flow of the superfluid

$$\mathrm{curl}\, \boldsymbol{v}_s = 0. \tag{4.8}$$

These equations lead to, among other things, equations for the propagation of first and second sound. First sound is an ordinary sound wave, exhibiting primarily fluctuations in the total density. Second sound is unique to helium II and represents primarily fluctuations in temperature. Neglecting friction terms and the coefficient of expansion, the velocities of first and second sound are

$$u_1^2 \approx \mathrm{d}\rho/\mathrm{d}\rho \qquad u_2^2 \approx TS^2\rho_s/C\rho_n \tag{4.9}$$

where C is the specific heat per unit mass.

4.2. Quantized vortices, rotation, attenuation of second sound by vortices

4.2.1. Quantized vortices and rotation. Equation (4.8) was at first thought to deny rotation to the superfluid fraction of helium II altogether, but Osborne (1950) found that the rotation of helium II was indistinguishable from that of helium I. Hall and Vinen (1956a, b) were able to show that, in a bucket of rotating helium II, the normal fluid rotates uniformly with the bucket but the superfluid vorticity $\omega = \mathrm{curl}\, v_s$ appears as a uniform array of discrete vortex lines parallel to the axis of rotation. For most purposes, a quantized vortex line can be thought of as a classical vortex line in the superfluid with a hollow core of radius a (about one ångstrom) and quantized circulation

$$\oint \boldsymbol{v}_s \cdot \mathrm{d}\boldsymbol{l} = \frac{h}{m} = \kappa \tag{4.10}$$

where the integration encircles the core, h is Planck's constant and m the mass of the helium atom: $\kappa \approx 9.97 \times 10^{-4}$ cm^2 s^{-1}. In a bucket rotating at angular velocity Ω radians per second the areal density of vortex lines, n_v, is the same as the line density L measured as length of line per unit volume (cm cm^{-3} = cm^{-2}), and is given by the ratio of the vorticity of solid body rotation to the quantum of circulation:

$$n_v = L = \frac{2\Omega}{\kappa} \approx 2000\Omega \text{ lines cm}^{-2}. \tag{4.11}$$

Vortex lines appear in more general flows as well, such as the flow between rotating cylinders and in the counterflow experiment described above. In the latter the vortex lines appear only after some critical heat flux q_c, and seem to be nearly randomly oriented with respect to the flow as suggested in the review article by Feynman. The vortices are sometimes described as a 'tangled mass', and densities up to the order of 10^5 cm^{-2} are easily generated. A book on the subject of quantized vortex lines has appeared (Donnelly 1991b).

Quantized vortices can be studied by attenuation of second sound (section 4.2.3), and by trapping of ions on the cores of the vortex lines (Donnelly 1991b). But it was Vinen's study of turbulent counterflow by means of the attenuation of second sound that led to a little known sequence of events in the discovery of quantized vortex lines. Vinen had obtained results by means of second sound attenuation which led him to believe the flow had become turbulent, and hence should have vorticity. Note that in Vinen (1957a) there is no reference to quantized vortices whatever. But in the second paper in the sequence of four papers on counterflow turbulence (Vinen 1957b), Vinen quotes Feynman's famous review article (Feynman 1955). However, in his discussion in section 6 of that paper, Vinen makes clear that the idea of vorticity in turbulent flow led directly to the famous Hall and Vinen experiments on rotating helium. Indeed, the Feynman paper appeared when the rotation experiments were under way. So we may conclude that quantized vortices were on their way to discovery by experiment about the same time as the theory was being worked out by Onsager (1949) and Feynman (1955).

The ideas behind quantized vortices and mutual friction developed rapidly in Vinen's mind, and by 1961 he had produced what is still one of the definitive reviews of the subject (Vinen 1961b).

4.2.2. Mutual friction in helium II: the Gorter and Mellink equations of motion. Gorter and Mellink (1949), motivated by experiments on pressure and temperature differences down narrow channels (see section 4.5.1), proposed that the extra dissipation above that owing to viscosity alone could be adequately represented by the addition of a 'mutual friction' term to the equations of motion. This idea was proposed long before the influence of quantized vortices on superflow was remotely realized. That realization had to await the work of Vinen and Hall. This term is now usually written as

$$F_{ns} = -\rho_s \rho_n A v_{ns}^2 v_{ns} \tag{4.12}$$

where $\boldsymbol{v}_{ns} = \boldsymbol{v}_n - \boldsymbol{v}_s$, $v_{ns} = |\langle v_{ns} \rangle|$, and A is a function of T (and in principle v_{ns}) and is of order 50 cm s^{-1} g^{-1}. The angular brackets denote spatial and temporal averages. This form of F_{ns} is useful for vortex turbulence work in counterflow channels, and is most frequently used in the steady state with time-averaged quantities.

In the case of rotating helium II, Hall and Vinen (1956a, b, 1961b) proposed

$$\boldsymbol{F}_{ns} = -(B\rho_n\rho_s/\rho)\hat{\boldsymbol{\Omega}} \times (\boldsymbol{\Omega} \times \boldsymbol{q}) - B'(\rho_n\rho_s/\rho)(\boldsymbol{\Omega} \times \boldsymbol{q}) \tag{4.13}$$

where $\boldsymbol{q} = (\boldsymbol{v}_s - \boldsymbol{v}_n)$ and $\hat{\boldsymbol{\Omega}} = \boldsymbol{\Omega}/|\boldsymbol{\Omega}|$. The component of mutual friction, then, in the direction of $\boldsymbol{q}$ is simply $\boldsymbol{F}_{ns} = B(\rho_s\rho_n/\rho)\boldsymbol{\Omega}q$, where $\boldsymbol{\Omega}$ is one-half the mean vorticity κL in the superfluid. The coefficients B and B' are called the mutual friction coefficients. The term with B leads to attenuation of second sound owing to scattering of rotons from quantized vortices (Samuels and Donnelly 1990) and the term with B' influences the splitting of second sound resonances in rotation experiments. The theory of mutual friction is discussed in depth in chapter 3 of Donnelly (1991b). The most current tabulations of the coefficients were obtained by Barenghi *et al* (1983a). Sometimes the B coefficients are replaced by α coefficients which are defined in equation (4.43). We shall discuss these relations in section 4.3 on the Hall–Vinen–Bekharevich–Khalatnikov equations.

4.2.3. Measurement of vorticity in helium II by second sound. Second sound absorption is a very sensitive tool which measures the length L of the quantized vortex line per unit volume, also referred to as a line density. The large cross section for vortices in second sound has its origin in the species change of rotons scattering in the flow field of a vortex line (Samuels and Donnelly 1990). The technique was introduced by Hall and Vinen, with Vinen publishing the

first results on turbulent flows (Vinen 1957a). The root-mean-square superfluid vorticity, ω_s, is defined by

$$\omega_s = \kappa L \tag{4.14}$$

where κ is the quantum of circulation (Donnelly 1991b). The lower level of sensitivity is dramatic: our least count in sensitivity is $L = 10\ \mathrm{cm}^{-2}$ leading to $\omega_s = 10^{-2}\ \mathrm{s}^{-1}$. On the higher end we have recorded values of ω_s to $50\,000\ \mathrm{s}^{-1}$ in turbulence produced by a towed grid (see figure 22) One can appreciate, however, that there is a limit to the use of second sound. The line density is deduced from the resonant amplitude A of second sound:

$$L = \frac{4\pi\,\Delta_0}{\kappa B}\left(\frac{A_0}{A} - 1\right) \tag{4.15}$$

where Δ_0 and A_0 are the resonant half-width and amplitude in the absence of vortex lines, owing to absorption of second sound by the walls, and B is the coefficient of mutual friction (Barenghi *et al* 1983a). In typical experiments at 1.65 K, $\Delta_0 = 8.77$ Hz, $B = 1.44$ and

$$\frac{A}{A_0} = \left(1 + \frac{\omega_s}{76.5}\right)^{-1} \tag{4.16}$$

so that for $\omega_s = 10^3\ \mathrm{s}^{-1}$, $A/A_0 = 7.1\times10^{-2}$, a few per cent of the original amplitude. The peak is also broadened since the product $A\Delta$ is known to be constant, at least for modest reductions in A. Broad peaks at low amplitudes are very hard to fit accurately, and so at a vorticity of this magnitude the second sound method becomes limited in its utility. Nevertheless, the range of five orders of magnitude of vorticity measurement is an impressive achievement.

Recently, Stalp (1998) has developed more accurate ways of analysing second sound attenuation data, and has produced a more general formula which reduces to the one developed by Vinen at low levels of attenuation.

One should note also that it is possible to measure vorticity in more than one direction. You (1993) was able to measure attenuation of second sound azimuthally and axially in a Taylor Couette apparatus

4.3. The HVBK equations of motion

The connection between superfluidity and fluid dynamics dates back to the *two-fluid model* of Landau and Tisza discussed in section 4.1. The link was reinforced by the discovery of quantized vortex lines in rotating helium. Attempts were then made to generalize the original two-fluid model into a complete set of fluid equations which is powerful enough to describe the motion of superfluid helium in the general case in which quantized vorticity is present in the flow (Hall and Vinen 1956a, b, Hall 1960, Vinen 1961b, Khalatnikov 1965, Hills and Roberts 1977). Much effort went into understanding various physical effects, such as mutual friction (Barenghi *et al* 1983a, b, c), which these equations should describe.

In section 4.2.1, we have seen that the simplest flow of helium II which contains vortex lines is solid-body rotation. This is an example of laminar vortex flow. There are only a few laminar vortex flows which have been investigated: flow in an annulus, Taylor–Couette flow, flow in a driven cavity. These flows have been studied using a generalization of the two-fluid equations which allows for non-zero, macroscopic superfluid vorticity ω_s. These equations are called the Hall–Vinen–Bekharevich–Khalatnikov (HVBK) equations, and generalize Landau's equations to include both the mutual friction and the tension force in the vortex lines which is responsible for vortex waves. The basic idea behind the HVBK equations is that we consider fluid particles large enough to be threaded by a large number of vortex lines which are essentially aligned along the same direction. These fluid particles are then treated as a continuum (see figure 1).

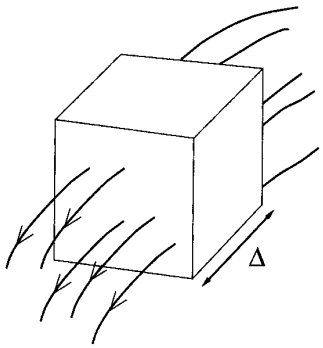

Figure 1. A fluid particle threaded by vortex lines in the HVBK model. The scale Δ of the particle of fluid is greater than the intervortex spacing.

Assuming incompressibility ($\nabla \cdot \boldsymbol{v}_n = 0\,, \nabla \cdot \boldsymbol{v}_s = 0$) the large-scale velocity field $\boldsymbol{v}_n$ and $\boldsymbol{v}_s$ obey the equations

$$\frac{\partial \boldsymbol{v}_n}{\partial t} + \boldsymbol{v}_n \cdot \nabla \boldsymbol{v}_n = -\nabla p_n + \nu_n \nabla^2 \boldsymbol{v}_n + \frac{\rho_s}{\rho} \boldsymbol{F}_{ns} \tag{4.17}$$

$$\frac{\partial \boldsymbol{v}_s}{\partial t} + \boldsymbol{v}_s \cdot \nabla \boldsymbol{v}_s = -\nabla p_s + T - \frac{\rho_n}{\rho} \boldsymbol{F}_{ns} \tag{4.18}$$

where p_n and p_s are effective pressures,

$$\nabla p_n = \frac{1}{\rho} \nabla P + \frac{\rho_s}{\rho_n} S \nabla T \tag{4.19}$$

$$\nabla p_s = \frac{1}{\rho} \nabla P - S \nabla T \tag{4.20}$$

$\nu_n = \eta / \rho_n$ is the normal fluid's kinematic viscosity,

$$\boldsymbol{T} = -\nu_s \boldsymbol{\omega}_s \times (\nabla \times \hat{\boldsymbol{\omega}}_s) \tag{4.21}$$

is the tension force,

$$\boldsymbol{c} = \boldsymbol{v}_n - \boldsymbol{v}_s - \nu_s \nabla \times \hat{\boldsymbol{\omega}}_s \tag{4.22}$$

$$\boldsymbol{F}_{ns} = (\tfrac{1}{2} B) \hat{\boldsymbol{\omega}}_s \times (\boldsymbol{\omega}_s \times \boldsymbol{c}) + (\tfrac{1}{2} B') \boldsymbol{\omega}_s \times \boldsymbol{c} \tag{4.23}$$

is the mutual friction force, B and B' are mutual friction coefficients,

$$\boldsymbol{\omega}_s = \nabla \times \boldsymbol{v}_s \tag{4.24}$$

is the (large-scale) superfluid vorticity, $\hat{\omega}_s = \omega_s / |\omega_s|$ and

$$\nu_s = (\kappa / 4\pi) \log(\Delta_{lines} / a) \tag{4.25}$$

is the vortex tension parameter, κ is the quantum of circulation and a is the vortex core parameter.

Equations (4.17) and (4.18) have three interesting limits. If $T \to T_\lambda$ then $\rho_s / \rho \to 0$ and (4.17) reduces to the classical viscous Navier–Stokes equation; if $T \to 0$ then $\rho_n / \rho \to 0$ and (4.18) reduces to the equation for a pure superflow; finally, if we set Planck's constant equal to zero, $T = 0$ and the pure superflow equation reduces to the classical inviscid Euler equation.

The HVBK equations have been used to study helium II inside a simple rotating cylinder and the Couette flow of helium II. In the core of the rotating cylinder the vortex lines are all parallel to the axis of rotation, so $\nabla \times \hat{\boldsymbol{\omega}}_s = 0$, there is no tension owing to bending and the HVBK equations assume a particularly simple form. In the core of Couette flow, on the contrary, the vortex lines can bend and one can really test the validity of the HVBK model.

4.4. Taylor–Couette flow in helium II

The potential of Taylor–Couette flow to investigate the dynamics of superfluid helium was recognized early on by Chandrasekhar and Donnelly (1958). Unfortunately, their pioneering attempt was premature and missed an important physical ingredient—vortex tension—which was not known at that time. Another unsuccessful attempt was carried out by Snyder (1974). Progress continued on the experimental side but, without a theoretical model, it was not possible to identify the observed instabilities with certainty, and attempts to compare results obtained using different techniques or different apparatus failed (Donnelly and LaMar 1988). A step forward occurred when Barenghi and Jones (1987) discovered the key role played by vortex tension. Barenghi's (1992) prediction of the critical velocity of the transition from Couette flow to Taylor vortex flow was confirmed by observations (Swanson and Donnelly 1991, Bielert and Stamm 1994) and contact between theory and experiments was achieved for the first time. The identification of this instability opened the way to understand flows and transitions observed at lower and higher velocities and stimulated more work on the problem. These advances established the general usefulness of the HVBK equations beyond the case of simple rotation for which they were formulated.

4.4.1. Classical Couette flow. In the classical Taylor–Couette problem a liquid of constant density ρ, and kinematic viscosity ν, flows between two concentric cylinders of inner radius R_1, outer radius R_2, gap $\delta = R_2 - R_1$ and height $h \gg \delta$. In the simplest configuration $\delta \ll R_1$, the outer cylinder is held fixed and the inner cylinder rotates at constant angular velocity Ω, measured by the Reynolds number $Re = \Omega R_1 \delta/\nu$.

The following sequence of flows and transitions takes places at increasing values of Ω. At small rotation rate the motion of the fluid is purely azimuthal around the inner cylinder (*Couette flow*). Using cylindrical coordinates r, ϕ, z the velocity is $v_0 = v_0\hat{\phi}$, where $\hat{\phi}$ is the unit vector along ϕ,

$$v_0 = Ar + B/r \tag{4.26}$$

$$A = -\Omega\eta^2/(1-\eta^2) \qquad B = \Omega R_1^2/(1-\eta^2) \qquad \text{and} \qquad \eta = R_1/R_2. \tag{4.27}$$

(It is important not to confuse the A and B coefficients with the coefficients of mutual friction introduced in section 4.2.2.) When Ω equals a critical value Ω_{1class} the viscous forces cannot hold back the unstable stratification of angular momentum any longer and Couette flow becomes unstable to axisymmetric perturbations of axial wavenumber $k = k_{1class} \approx 3/\delta$. The new flow pattern has the form of toroidal cells of wavelength $\lambda = 2\pi/k \approx 2\delta$ superimposed upon the azimuthal motion (*Taylor vortex flow*). When a second critical velocity Ω_{2class} is reached, the boundaries of the Taylor cells start to oscillate, the flow pattern loses its axial ($m = 0$) symmetry and becomes time dependent with non-zero azimuthal wavenumber m (*wavy modes*). At higher velocities other transitions occur and the flow becomes more complex and eventually turbulent, but Taylor cells are still visible.

4.4.2. Appearance of the first vortex line. At small values of Ω, helium II is in a vortex-free state. Vortex lines appear at a critical angular velocity Ω_0. The nucleation of the first vortex line is still a major unsolved problem of superfluidity and requires a microscopic quantum description, but some progress has been made using more general arguments. The first argument, introduced by Hall and Vinen (1956b), and further developed by Donnelly and Fetter (1966), is based on thermodynamics and states that the first vortex appears when $F - \Omega L$ is a minimum, where F is the free energy and L is the angular momentum. The background of this assertion is contained, for example, in sections 26 and 34 of Landau and Lifshitz (1969).

Swanson and Donnelly (1987) applied the theory to Couette flow and found that (by symmetry) the first row of vortices should appear in the gap at the critical velocity

$$\Omega_0^* = (2\kappa/\pi R_2\delta)[\ln(2\delta/\pi a_0) + \tfrac{1}{4}]. \tag{4.28}$$

The measured critical velocities, however, are two to three times higher and show a strong temperature dependence which is absent in Ω_0^* (Swanson and Donnelly 1991, Bielert and Stamm 1994).

The second argument, proposed recently by Jones *et al* (1995), is based on fluid dynamics rather than thermodynamics. Consider a transition from a state characterized by the velocity fields v_n and v_s just after the transition. The transition is possible only if the energy of the configuration before transition exceeds the energy after, i.e. if

$$E_n + E_s > \tilde{E}_n + \tilde{E}_s. \tag{4.29}$$

From the configurations of the proposed transition one can calculate $E_n + E_s$ and $\tilde{E}_s$. To find $\tilde{E}_n$ requires some assumptions about the nature of the transition. The first assumption is that the appearance of a vortex happens on a very rapid quantum timescale ($\approx a_0^2\kappa = 10^{-13}$ s) so that momentum is conserved *locally* at each point in the fluid. The second assumption is that, at the moment of creation, the vortex is not coupled to the walls, so that no angular momentum is transferred to them. Immediately after the formation of the vortex, adjustments to the pressure distribution, and hence to the momentum distribution, will occur on the sound speed timescale. Further adjustments will occur on the viscous diffusion timescale (typically minutes). The quantum timescale is much faster than these effects, so that they do not affect the process of formation, but only what is subsequently observed. Local conservation of momentum then implies $\rho_n v_n + \rho_s v_s = \rho_n \tilde{v}_n + \rho_s \tilde{v}_s$. When this theory is applied to Couette flow it is found that, as Ω is gradually increased, the first transitions involve the creation of quanta of irrotational superfluid motion. When Ω reaches the critical value

$$\Omega_0 = (1 + \rho_s/\rho_n)\Omega_0^* \tag{4.30}$$

the strength of the virtual vortex is large enough that the vortex-free state becomes unstable and real vortex lines appear. This result agrees with both the magnitude of the observed critical velocity and its temperature dependence in the temperature range $1.85 < T < T_\lambda$. Below $\sim$1.85 K the theory fails, but this is expected, because the mean free path of the excitations which make the normal fluid becomes as large as the container and local conservation of momentum does not apply. What happens below 1.85 K is therefore still an open question. Further support for the new theory comes from the observation of predicted hysteresis effects (Mathieu *et al* 1976).

4.4.3. Azimuthal Couette flow. If Ω is increased above Ω_0, more and more rows of vortices appear quickly, until a uniform array of vortices aligned in the z-direction fills the gap. The small-scale flow pattern is very complicated, but the large-scale superfluid velocity field is the same as the Couette profile v_0 of the normal fluid. A suitable description of this large-scale flow which ignores the individual vortex lines is the HVBK model.

Applied to Couette flow, equations (4.17) and (4.18) admit the isothermal Couette solution $v_n = v_s = v_0$ which corresponds to an array of vortex lines aligned along the z-direction with areal density

$$n_0 = 2|A|/\kappa. \tag{4.31}$$

4.4.4. Transition from Couette flow to Taylor vortex flow. When reaches a critical value Ω_1, the Couette state becomes unstable to axisymmetric perturbations of axial wavenumber k_1 and toroidal motion appears (Barenghi 1992, Henderson and Barenghi 1994). Ω_1 is strongly temperature dependent. In the high-temperature limit $\Omega_1 \rightarrow \Omega_{1class}$ because helium II $\rightarrow$ helium I. To understand the instability at lower T it is important to remember that in the classical case the stability boundary in the (Ω, k) plane looks like a parabola with vertex at the base, $k = k_{1class} \approx 3/\delta$ and $\Omega \rightarrow \Omega_{1class}$; that is to say, the Taylor cells are square. Consider now helium II in the limit $T \rightarrow 0$. It can be shown (Barenghi and Jones 1987) that the Couette solution of the pure superflow equation is unstable to long wavelength perturbations of the vortex lines and the stability boundary looks like a parabola with vertex at the origin ($\Omega_1 \rightarrow 0$ as $k \rightarrow 0$). In practice the cylinders have finite height so that the critical wavenumber is not $k = 0$ but some small finite k_{min}. What happens at a temperature between 0 and T_λ depends on the relative proportions of ρ_n and ρ_s. Just below T_λ, $\rho_n/\rho \leqslant 1$ and helium's dynamics is dominated by the normal fluid, which, since $\rho_s/\rho \ll 1$ in (4.17), behaves almost like a classical Navier–Stokes fluid. When $\Omega = \Omega_{1class}$ the normal fluid would like to overturn Couette flow into Taylor cells on the length scale $\lambda = 2\pi/k_{1class} \approx 2\delta$, but the vortex lines are very stiff on this short scale—remember that the stability boundary for a pure superflow increases rapidly with k. A compromise is reached between the two effects and the instability sets in at higher velocity ($\Omega_1 > \Omega_{1class}$) and smaller wavenumber ($k_1 < k_{1class}$), thus making helium II in this region more stable than helium I. If the temperature is reduced the balance is struck at lower Ω_1 more in favour of the superfluid: the Taylor cells appear at $\Omega = \Omega_{1class}$ and are very long axially. For $T < 2$ K the critical velocity drops rapidly because of the rapid decrease of the normal fraction ($\rho_n/\rho \approx 0.5$ at $T \approx 2$ K).

The experiments of Swanson and Donnelly (1991) and Bielert and Stamm (1993) confirm this scenario.

The HVBK equations have also been tested in the axisymmetric nonlinear regime $\Omega > \Omega_1$ (Henderson and Barenghi 1994, Henderson *et al* 1995). It is found that the structure of the Taylor cells is different from classical Taylor vortex flow. The observed values of the torque induced on the outer cylinder (Donnelly 1959) compare well with the theoretical predictions. Estimates of the second sound attenuation are more difficult, but still in order of magnitude agreement with the measurements.

4.4.5. Wavy modes. Wolf *et al* (1981) observed many transitions at large rotational velocity which have not been identified yet. They are possibly related to non-axisymmetric modes of the Couette solution which become unstable for $\Omega > \Omega_1$ (Barenghi and Jones 1988). To make contact with the experiments it will be necessary to perform a proper linear stability analysis of nonlinear Taylor vortex flow with respect to $m \neq 0$ modes. This regime is very much open to further work.

4.4.6. Turbulent Couette flow. Bielert and Stamm (1994) found that the turbulent Couette flow of helium II ($\Omega \approx 40\Omega_1$) is similar to classical turbulence in two respects: axisymmetric Taylor cells are still visible, even if the flow inside each cell is turbulent, and the Taylor cells are square, not elongated axially. Other experiments confirm the similarity between the isothermal turbulent flow of helium II and classical turbulence (Barenghi *et al* 1995a).

There is no direct theoretical evidence that the normal fluid and the superfluid are coupled at high Reynolds numbers, because we do not know whether the HVBK equations, which have been successfully tested at small Reynolds number, are still applicable in the turbulent regime. This is still an issue open to investigation. Nevertheless, we can try to extrapolate what we

know at the relatively small values of Reynolds number used in Taylor–Couette experiments. The HVBK equations lead us to consider the relative importance of the tension force $\boldsymbol{T}$ and the mutual friction force $\boldsymbol{F}_{ns}$ in the superfluid equation of motion, at high Reynolds number. For if $\boldsymbol{T}$ is small compared to $\boldsymbol{F}_{ns}$ then the only significant forces acting on the superfluid are the pressure and mutual friction. The pressure force on the superfluid is the same as that on the normal fluid and mutual friction will have the effect of trying to lock up the two fluids on sufficiently large length scales. Consequently, a small value of the ratio of $|\boldsymbol{T}|/|\boldsymbol{F}_{ns}|$ would support the concept.

We assume that the temperature T is high enough that helium's dynamics are essentially dominated by the normal fluid equation, and the superfluid equation acts only as a correction. In Couette flow, for example, at high T, the normal fluid equation determines both the flow's pattern (Taylor cells) and the magnitude of the critical Reynolds number.

Now let λ be the length scale of the channel, V the magnitude of the velocities and Ω_s the amount of superfluid vorticity. Then $\boldsymbol{T} \sim \nu_s \Omega_s/\lambda$ and $\boldsymbol{F}_{ns} \sim \rho/\rho_n \Omega_s (V - \nu_s/\lambda)$ if we neglect the small B' term. Apart from a very small region in the close vicinity of the lambda point, the mutual friction coefficient B is of order unity, and the ratio of the magnitudes of the tension force and the mutual friction force reduces to

$$\frac{|\boldsymbol{T}|}{|\boldsymbol{F}_{ns}|} \approx \frac{\beta\rho/\rho_s}{Re(1-(\beta/Re))} \approx \frac{\rho_n}{\rho}\frac{1}{Re}. \tag{4.32}$$

Here $\beta = \nu_s/\nu_n$ is a parameter of order unity at typical temperatures, and we define the Reynolds number as $Re = V\lambda/\nu_n$. It is apparent from (4.32) that at large Reynolds numbers $|\boldsymbol{T}|/|\boldsymbol{F}_{ns}| \to 0$ and thus the vortex tension term is negligible compared to the mutual friction. We conclude that the superfluid is essentially dragged along by the normal fluid via mutual friction.

4.4.7. Rotations of the outer cylinder. The stability of Couette flow under rotation of the *outer* cylinder, on the contrary, is still an unsolved problem. Unlike what happens in a classical fluid, for which rotations of the outer cylinder stabilize Couette flow, helium II undergoes a transition if the velocity of the outer cylinder exceeds a critical value. Heikkila and Hollis Hallet (1955) and Barenghi and Jones (1987) discovered that at $T = 0$ *any* rotation of the outer cylinder is destabilizing, but a study of the problem at the finite temperatures relevant to the experiments is still missing. Flow between counter rotating cylinders is discussed by Barenghi *et al* (1995b).

4.4.8. Couette flow at small aspect ratio. If the height of the Couette apparatus is reduced to the gap's size, one obtains a simple cavity. Recently, Henderson and Barenghi (1999) studied the flow of helium II in this simple configuration using the HVBK model. They found the surprising result that the normal fluid, at some values of parameters, flows in the opposite direction to what a denser fluid would do.

4.5. Counterflow turbulence

4.5.1. Leiden measurements. The early history of counterflow turbulence begins with investigations at Leiden University on the thermal conductivity of liquid helium. Keesom and Keesom (1936) measured the thermal conductivity of helium I in the apparatus of figure 2(*a*). The liquid was contained in a cylindrical layer L of diameter 3.6 cm and depth 0.5 cm. The top and bottom of the cell consisted of copper blocks A and B, each containing a heater and thermometer. At $T = 3.3$ K the authors obtained a thermal conductivity comparable to that of gases at ordinary temperatures. The thermal conductivity of helium II, on the other hand, is so

great that a capillary tube must be used to observe a temperature gradient. The first systematic measurements were by Keesom *et al* (1938) using the apparatus of figure 2(*b*).

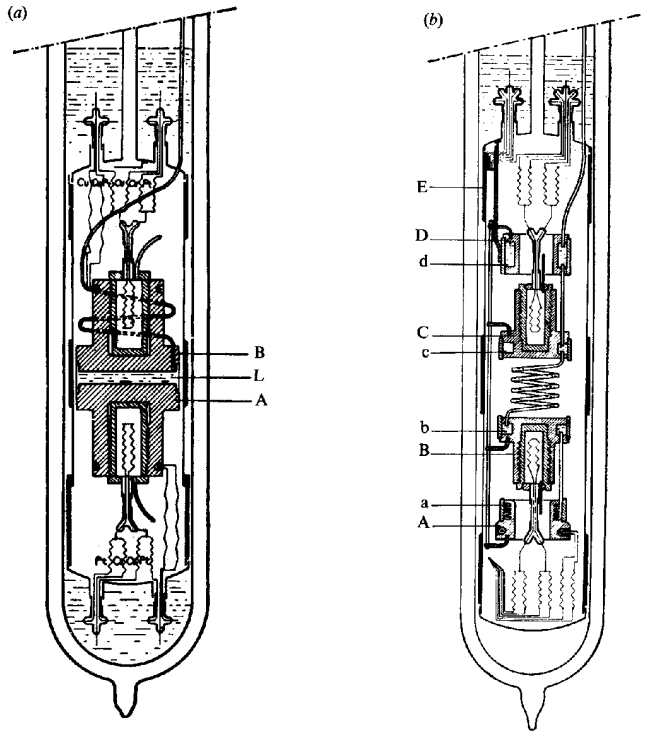

Figure 2. Apparatus for determining: (*a*) the thermal conductivity of helium I (Keesom and Keesom 1936); (*b*) the relationship between heat flux and temperature gradient in helium II (Keesom *et al* 1938). The components are discussed in the text.

A, B, C and D are copper pieces containing chambers a, b, c and d filled with liquid helium through metal capillaries. Capillaries of different width and length were used between B and C. B and C also contained thermometers and a heater was attached to A. The authors found that the heat conductivity has a pronounced maximum at 1.7–2.0 K with conductivity as high as 810 cal $^{\circ}C^{-1}$ cm^{-1} s^{-1}, i.e. more than 800 times that of copper at room temperature, and 1.3×10^7 the value obtained for helium I. Keesom *et al* called helium II 'supra-heat conducting', with good justification.

It is interesting that the devices illustrated in figure 2 are in use today in more or less the same form. The helium I cell appears today as a Bénard convection cell (see section 3.2 above). The so-called 'counterflow' apparatus of figure 2(*b*) still represents one of the most important and fundamental techniques for studying the flow of helium II: a heat source, and thermometers to measure the temperature gradient.

Readers interested in following the evolution of experiments on counterflow turbulence over the years might consult Atkins (1959), Wilks (1967), Donnelly (1967), Tough (1982), Swanson and Donnelly (1985) and Donnelly (1991b).

Much of the study of quantum turbulence is done in steady-state counterflow. The time and cross sectional averages of (4.4) and (4.5) in steady state (the 'mutual friction approximation')

are, to first order,

$$0 = -(\rho_s/\rho)\langle\nabla P\rangle + \rho_s S\langle\nabla T\rangle - \langle \boldsymbol{F}_{ns}\rangle \tag{4.33}$$

$$0 = -(\rho_n/\rho)\langle\nabla P\rangle - \rho_s S\langle\nabla T\rangle + \langle \boldsymbol{F}_{ns}\rangle + \eta\langle\nabla^2 \boldsymbol{v}_n\rangle \tag{4.34}$$

where brackets denote time and cross sectional averages. Adding (4.33) and (4.34), we find

$$\langle\nabla P\rangle = \eta\langle\nabla^2 \boldsymbol{v}_n\rangle \tag{4.35}$$

which suggests that the pressure gradient ∇P in turbulent superflow is not much different to that in laminar (Poiseuille) flow. This is known to be roughly true, and is called 'the Allen and Reekie rule'. The Allen and Reekie rule is not quite obeyed, as detailed in section 4.1 of the review by Tough (1982), but it did prompt Gorter and Mellink (section 4.2.2) to propose mutual friction!

With a laminar mean flow assumption, we have for the pressure gradient

$$\nabla P_L = -\frac{G\eta \boldsymbol{v}_n}{d^2} \tag{4.36}$$

where G is a factor know theoretically for Poiseuille flow for each channel shape and d is the channel size. The thermodynamic potential gradient per unit mass, usually called the chemical potential in the helium II literature, vanishes in laminar flow,

$$\nabla \mu_L = -S\nabla T_L + \frac{\nabla P_L}{\rho} = 0 \tag{4.37}$$

consistent with dissipationless flow for the superfluid. Thus the laminar flow temperature gradient is

$$\nabla T_L = \frac{\nabla P_L}{\rho S} = -\frac{G\eta v_n}{\rho S d^2}. \tag{4.38}$$

In turbulent flow, the total temperature gradient is

$$\nabla T = \nabla T_L + \nabla T_T \tag{4.39}$$

where ∇T_T is, neglecting the increase in ∇P above the laminar value,

$$\nabla T_T = \frac{\boldsymbol{F}_{ns}}{S\rho_s} \tag{4.40}$$

and since $\boldsymbol{F}_{ns}$ varies roughly as v_{ns}^3, the neglect of the extra pressure gradient becomes quantitatively reasonable for large flow rates. The chemical potential gradient is given by

$$\nabla \mu = -\frac{\boldsymbol{F}_{ns}}{\rho_s}. \tag{4.41}$$

This shows that dissipation owing to vortices produces a direct change in chemical potential.

The connection of the mutual friction coefficients to line length per unit volume may be seen by a simple analogy. In uniform rotation, from (4.41), the dissipative term of F_{ns} parallel to v_{ns} has the magnitude $B\rho_s\rho_n\kappa L/2\rho$, where κL is the vorticity 2Ω in steady rotation. For turbulent flow the assumption is that mutual friction acts in the same manner on each segment of vortex line in a tangle as it does on an array produced by rotation, but that in second sound attenuation, for example, an average of one-third of the vortex line segments in the tangle will be oriented parallel to the second sound propagation direction and not detected. Thus for isotropically-oriented vortex lines, the magnitude of the dissipative part of the mutual friction term can be written as

$$F_{ns} = -\frac{B\rho_s\rho_n\kappa}{2\rho}\frac{2}{3}L_0 v_{ns} \tag{4.42}$$

where $L_0 = \langle L \rangle$. For a more careful discussion of the relationship between second sound measurements and the properties of the tangle, see Swanson and Donnelly (1985) or Stalp (1998).

We note here for future reference that in place of B and B' authors often use

$$\alpha = B\rho_n/2\rho \qquad \alpha' = B'\rho_n/2\rho. \tag{4.43}$$

Indeed α can be used as a convenient measure of temperature. The upper and lower abscissae of figure 7 show the correspondence between T and α.

4.5.2. Vinen's theory. A model for the dynamics of the tangle of quantized vortex lines, developed from the ideas of mutual friction, was introduced by Vinen in a classic series of papers (Vinen 1957a, b, c, 1958). This theory considers a spatially homogeneous distribution of vortex lines whose time rate of change is determined by competing growth and decay processes. Vinen derived the growth term by dimensional analysis and modelled the decay process after the decay of classical turbulence in the Kolmogorov cascade. He obtained

$$\frac{\mathrm{d}L}{\mathrm{d}t} = \chi_1 \frac{B}{2}\frac{\rho_n}{\rho} v_{ns} L^{3/2} - \frac{\chi_2 \kappa}{2\pi} L^2 \tag{4.44}$$

where χ_1 and χ_2 were undetermined parameters at the time.

In a steady state $\langle \mathrm{d}L/\mathrm{d}t \rangle = 0$ and the equilibrium line density is

$$L_0 = \gamma^2 v_{ns}^2 \tag{4.45}$$

where $\gamma = \pi B \rho_n / \kappa \rho \chi_2$. The v_{ns}^2 dependence of L_0 predicted by Vinen's model is roughly correct above the critical heat flux (see section 4.5.4). γ, which contains the temperature dependence, had to be determined experimentally since χ_1 and χ_2 were not well known.

If v_{ns} is set to zero, the free decay of the tangle is described by

$$L(t) = \frac{L_0}{1 + L_0(\chi_2 \kappa/2\pi)t} \tag{4.46}$$

where L_0 is the initial vortex line density. It is known that this scaling does not persist at large times (see figure 23 and section 4.7.3).

Writing $L/L_0 = \ell$, we have from equation (4.44)

$$\frac{\mathrm{d}\ell}{\mathrm{d}t} = K_1 v_{ns}^2 \ell^{3/2}(1 - \ell^{1/2}) \tag{4.47}$$

where

$$K_1 = \frac{B^2}{4}\frac{\chi_1^2}{\chi_2}\left(\frac{\rho_n}{\rho}\right)^2 \frac{m}{\hbar}. \tag{4.48}$$

Applying this equation to the build-up of mutual friction when a steady heat current is suddenly switched on, Vinen noted that ℓ is simply equal to the ratio of the mutual friction at any instant to the final equilibrium value of the mutual friction. Therefore, from an experimental curve showing the build-up of mutual friction when a heat current is switched on, it was possible to deduce values of $\mathrm{d}\ell/\mathrm{d}t$ and ℓ as a function of time for a given value of v_{ns}, and these values could then be used to test the validity of equation (4.47). In practice, plots were made of $\mathrm{d}\ell/\mathrm{d}t$ against $\ell^{3/2}(1 - \ell^{1/2})$ which were found to be straight lines within the experimental error, and this constitutes experimental evidence in favour of the dependence of $\mathrm{d}\ell/\mathrm{d}t$ on ℓ indicated by equation (4.47). From the slopes of these lines, values of $K_1 v_{ns}^2$ were obtained. For a given temperature these values of $K_1 v_{ns}^2$ are found to be proportional to v_{ns}^2, so that the form of dependence of $\mathrm{d}\ell/\mathrm{d}t$ on v_{ns}^2 indicated by equation (4.47) was also confirmed.

Schwarz (1988) (see section 4.6) has used the laws of vortex dynamics to study the dynamical balance between growth and decay and finds an equation analogous to Vinen's. The advantage of Schwarz's derivation is that χ_1 and χ_2 are no longer unknowns, but are derived directly from the laws of vortex dynamics.

A comparison between the decay of counterflow turbulence and towed grid turbulence is shown in section 4.8.3.

4.5.3. Critical heat flux. Vinen (1958) observed that a critical heat flux, and hence a critical average counterflow velocity v_c is necessary to generate an observable quantity of vortex line. He did this with second sound attenuation, and the existence of a critical counterflow velocity has been confirmed since by second sound attenuation, temperature and chemical potential gradients, as well as ion trapping (Tough 1982).

4.5.4. Dependence of line density on counterflow velocity. The dependence of the average line L_0 upon v_{ns} near critical is complicated, but observers generally agree that beyond the critical region

$$L_0 \approx \gamma^2 (v_{ns} - v_0)^2 \tag{4.49}$$

where γ and v_0 are functions of temperature (do not confuse v_0 with v_c). The precise values of γ and v_0 have been the subject of controversy (Donnelly *et al* 1981), but the turbulent state classification of Tough (1982) described in section 4.5.5, the recent work on scaling (Schwarz 1988, Swanson and Donnelly 1985) described in sections 4.5.6 and 4.5.7, and the measurement of the tangle anisotropy described in section 4.5.9 combine to resolve apparent experimental discrepancies.

4.5.5. Tough classification of turbulent states. Tough (1982) has analysed the vast quantities of steady, uniform counterflow data and found that there is one feature of the channel geometry which is crucial in determining the phenomena, the cross sectional aspect ratio. (Apparently the channels used are long enough for the length-to-width ratio to be of little importance, at least well beyond critical). For low-aspect-ratio channels (e.g. nearly square or circular) there are two turbulent states, state TI at low heat fluxes and state TII at high heat fluxes, which are separated by a rather complicated transition (see section 4.5.13) and have different characteristic values of γ. For high-aspect-ratio channels there is only one turbulent state, state TIII, which has values of γ similar to state TII. Tough also designated the turbulence in pure superflow as state TIV, a state which has mass flow and presumably a flat velocity profile. From the latest data (Opatowsky and Tough 1981) it appears that γ in state TIV agrees quantitatively with γ in state TII (Awschalom *et al* 1984, figure 1b). The critical velocities for these different flows are designated v_{c1}, v_{c2}, etc.

4.5.6. Vortex dynamics and scaling. For many years scaling in counterflow turbulence was unknown. This is in part due to the fact that there is no mass flow in counterflow experiments and familiar ideas such as the Reynolds number, being the ratio of inertia to dissipation, are unavailable. The topic is subtle, but is summarized in section 7.2.2 of Donnelly (1991b), based on original work by Swanson and Donnelly (1985). What emerges is a dimensionless tangle-averaged logarithmic factor

$$l_0 \approx -\ln(a L_0^{1/2}). \tag{4.50}$$

Defining $\beta = \kappa l_0/4\pi$ (with dimensions of kinematic viscosity), the dimensionless applied counterflow velocity V (analogous to a Reynolds's number) upon which tangle properties will depend is

$$V = \frac{v_{ns} d}{\beta}. \tag{4.51}$$

4.5.7. Implications of scaling. There are two major implications of the scaling of tangle properties with V, i.e. the scaling of critical velocities with channel size and the relationship between line density and counterflow velocity (for high velocities). This relationship has further implications, for example the scaling of γ with channel size and the temperature and heat flux dependence of the Gorter–Mellink law exponent.

We can define a dimensionless critical velocity from (4.51),

$$V_c \equiv \frac{v_c d}{\beta_c} \tag{4.52}$$

where v_c and β_c are the values of v_{ns} and β at the critical velocity. In figure 3 we show measurements of $v_{c2}d$, the second critical velocity in small aspect ratio channels scaled by the channel size (ignoring the logarithmic parameter), and of v_{c2}, i.e. the same data scaled according to (4.52). We can see substantial improvement in agreement between measurements in various sized channels with the inclusion of the logarithmic parameter. Similar improvements in agreement can be seen for other critical velocity measurements, see Swanson and Donnelly (1985).

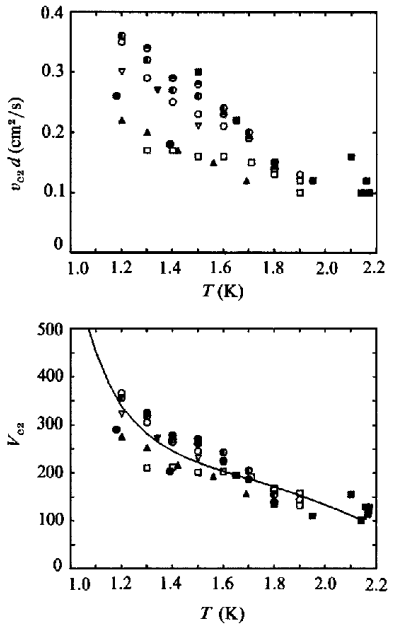

Figure 3. Second critical velocity in small aspect ratio channels at several temperatures as determined by various investigators. The upper plot is scaled by channel size, whereas the lower plot includes the logarithmic parameter as in (4.52). Until recently there were no theories of this transition. However, recently Melotte and Barenghi (1998) have argued that the transition TI–TII indicates the beginning of turbulence in the normal fluid, so that TII is a region of turbulence in the entire fluid.

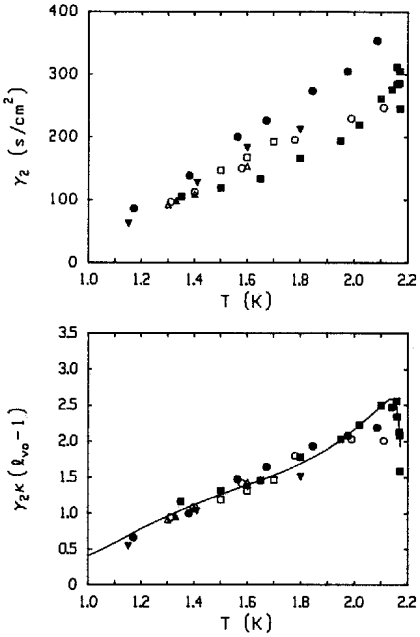

Figure 4. γ_2 as a function of temperature. The upper plot shows γ_2 and the lower plot shows γ_2 scaled by the implicit channel-size dependence after Swanson and Donnelly (1985).

At high counterflow velocities, the boundary region becomes less important for determining average tangle properties, and L_0 need not be proportional to d^{-2}. Then (4.52) can be written as

$$L_0^{1/2} = \frac{u_i}{\beta_c} v_{ns}. \tag{4.53}$$

The dependence of L_0 on v_{ns}^2 can thus be derived simply from the scaling of vortex dynamics in the approximation that the logarithmic parameter is constant. Inclusion of the logarithmic parameter gives a remarkably good fit to the data, as can be seen in figure 5.

We can make a linear approximation of (4.53) about some $v_{ns} = v_{ns0}$, where l_0 has the value l_{v0}, finding

$$L_0^{1/2} = \gamma(v_{ns} - v_0) \tag{4.54}$$

where $\gamma = 4\pi u_i/\kappa c(l_{v0} - 1)$ and $v_0 = v_{ns0}/l_{v0}$, see figure 4. The parameter v_0 which appears in this expression for L_0 is the same as the v_0 appearing in (4.49). It has no physical significance. Its presence arises naturally due to logarithmic scaling, and its value depends on where one makes the linear approximation as well as on temperature and channel size. Below we will use a nonlinear power-law approximation to (4.5.3), $L_0^{1/2} = bv_{ns}^n$, which is good over a much wider range than the linear approximation.

The logarithmic parameter also has important implications for the Gorter–Mellink relationship between the temperature gradient and the applied heat flux. Let us amend the usual Gorter–Mellink rule to write

$$\nabla T_T = -F_{ns}/S\rho_s \propto q^m \tag{4.55}$$

where $m = 3$ is the traditional value. Swanson and Donnelly (1985) show that it is possible to use a nonlinear power approximation to (4.53),

$$L^{1/2} \propto v_{ns}^n \tag{4.56}$$

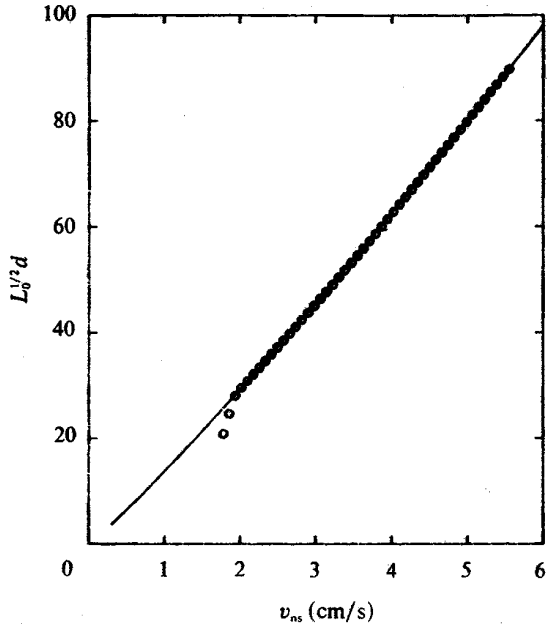

Figure 5. $L_0^{1/2}d$ as a function of v_{ns} at 1.7 K. The data are from Martin and Tough (1983). The line represents (4.53). For details see Swanson and Donnelly (1985). The scaling shown here is also implicit in the Schwarz simulations as discussed in Schwarz (1988), which gives not only the scaling but also the magnitude of the mutual friction.

which is valid over a wider velocity range than the approximation (4.54). This leads to the result $m = 2n + 1$ in (4.55). Swanson and Donnelly (1985) go on to show that (4.55) is a good approximation about some heat flux q_0, with m a function of temperature and q_0 as shown in figure 6. These values are consistent with a variety of experiments (Ahlers 1969, Bon *et al* 1978, Swanson and Donnelly 1985) that have roughly determined m. The theory leading to this result breaks down as m grows, essentially because the core becomes comparable to $L_0^{1/2}$, but it is probably satisfactory while m is less than 4.

4.5.8. Axial homogeneity of vortex line density in a counterflow channel. The vortex line density in turbulent counterflow is axially homogeneous in a properly designed channel (see section 4.2). The axial homogeneity is consistent with the Vinen equations which imply that the tangle is sustained by the local value of v_{ns}. Further evidence for local creation has been provided by shock-wave experiments of Barenghi (1982). Barenghi's experiments, done by attenuation of second sound allowed him to conclude that vortex lines can be created by shock waves and that the velocity at which the initiation of vorticity is propagated is the velocity of second sound.

4.5.9. Transverse homogeneity and anisotropy of the tangle. Awschalom *et al* (1984) have reported that the vortex line density L is independent of transverse position over at least 80% of a channel of width 1 cm. This observation was made by ion trapping in the cores of quantized vortices. In the same experiment, it is reported that the normal fluid velocity profile is uniform over at least 80% of the channel and the normal fluid is certainly not in Poiseuille flow. Indeed, it appears that turbulent counterflow is more or less 'plug flow'.

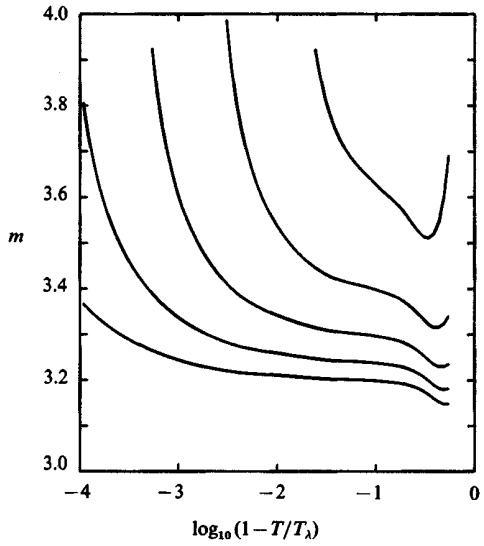

Figure 6. The Gorter–Mellink m as a function of temperature and heat flux. From the top of the figure the lines are for heat fluxes of 10 W cm^{-2}, 1 W cm^{-2}, 0.1 W cm^{-2}, 10 mW cm^{-2}, and 1 mW cm^{-2}. After Swanson and Donnelly (1985).

The standard assumption since the work of Vinen (1957a, b, c, 1958) has been that the vortex line density is isotropic. We find by simultaneous transverse and axial measurements that the line density distribution is substantially flattened in a direction perpendicular to the axial flow (Wang *et al* 1987). Figure 7 shows the ratio L_T/L_A, which would be unity for an isotropic distribution and 0.5 if all of the lines were perpendicular to the flow. Here L_T is the line density measured transverse to the flow axis, and L_A is the line density measured parallel to the counterflow axis.

4.5.10. Drift of the tangle. Vinen (1957c) assumed that the vortex lines, being an excitation of the superfluid would have velocity v_s and thus move toward the heater. There have been some early reports that the tangle moves toward the cold side of the channel. These are probably wrong. Barenghi *et al* (1983a, b, c) suggested that combined temperature gradient and second sound measurements could yield the ratio

$$|\langle v_L - v_s\rangle|/|\langle v_n - v_s\rangle| = v_{LS}/v_{ns}. \tag{4.57}$$

This measurement was carried out by Wang (1987), who found $v_L \approx v_s$ for temperatures in the range 1.27–2.1 K (see figures 7 and 8), in accordance with Vinen's original assumption.

4.5.11. Fluctuations. The intrinsic fluctuations of the vortex line density are quite weak, and early reports of the nature of the fluctuations were probably wrong. On the other hand, the Vinen equations can be interpreted in a way which gives the response to induced fluctuations of v_{ns}. An experiment to test this prediction by Barenghi *et al* (1982) was carried out using a noise generator to modulate the heater driving the flow. Their results fully confirm the predictions of Vinen's equations except perhaps very close to the lambda transition.

4.5.12. Combined rotation and counterflow. Combined rotation and heat flow is a relatively new area of investigation. Prior to the investigation discussed in this section it was assumed

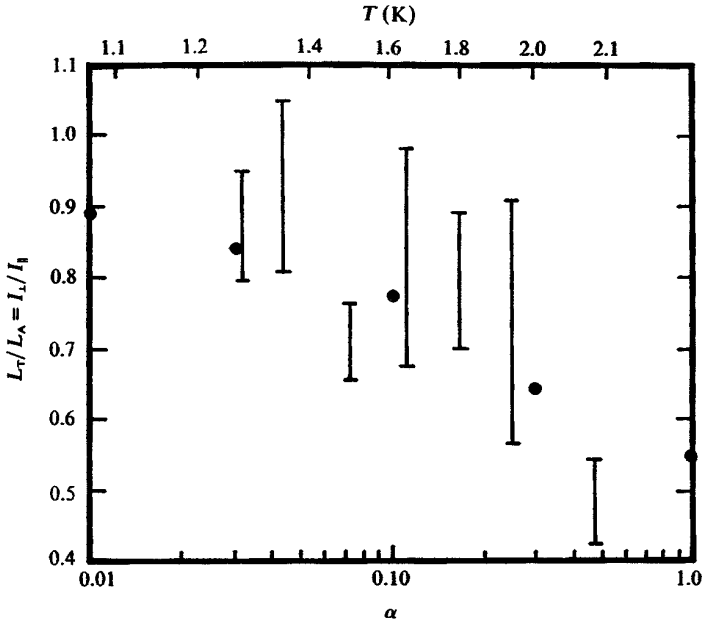

Figure 7. The ratio L_T/L_A of line density measured as a function of temperature (Wang *et al* 1987). These results were also calculated by Schwarz (1988) from simulations as shown by the full circles.

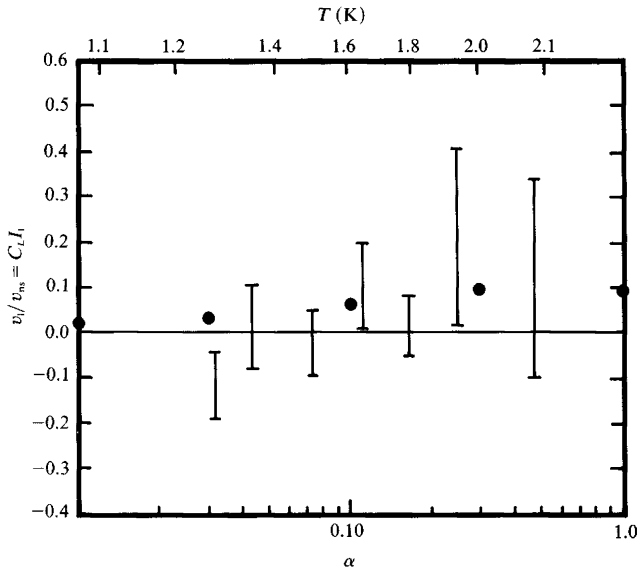

Figure 8. The ratio v_{Ls}/v_{ns} as a function of temperature. The bars represent the data of Wang *et al* (1987) (the range shown is three standard deviations). The full circles are the predicted vortex drift velocities by Schwarz (1988).

(from earlier experiments) that the ordered array of vortex lines produced by steady rotation and the disordered tangle produced by counterflow preserved their identities in a combined

experiment. Measurements at Oregon with improved sensitivity by Barenghi *et al* (1983c) showed that the picture just described is far from true. The observations consisted of measuring the amount of vortex line present owing to counterflow or rotation alone using second sound attenuation, and comparing the observed line density with what would be expected if the two sources of vorticity simply added. The results are complicated, but appear to be relatively simple in two limits.

(i) Limit of large line density L_H due to heat, slow rotation. Here the effect of rotation is not simply to add line density $L_R = 2\Omega/K$. Instead the tangle appears to be polarized to accomplish the rotation. The effective polarization increases with rotation Ω by analogy to a gas of magnetic dipoles in a magnetic field. The results scale with L_R/L_H by analogy to $\mu H/kT$. Thus rotation appears to produce alignment in the tangle, as does a magnetic field for dipoles, and L_H appears to play the role of disordering heat bath in the statistical mechanics of superfluid turbulence.

(ii) Limit of fast rotation and small axial heat flux. Any rotation eliminates the critical velocity v_c. In this limit two critical counterflow velocities appear, v_{c1} and v_{c2}, which scale as $\Omega^{1/2}$. The first appears to correspond to the Donnelly–Glaberson instability (see section 4.7.5): excitation of helical waves by the counterflow on the vortex lines induced by rotation. The second appears to be a transition to turbulence, with the rotation-induced array becoming a vortex tangle.

4.5.13. Dynamics of the TI–TII transition. Recently there has emerged an important insight into the nature of the TI–TII transition in circular pipes. TI and TII are superfluid vortex tangles of much different vortex line densities, TII being considerably larger. We have known since the pioneering experiments of Vinen that if the heat flux q exceeds a critical value, a vortex tangle is created. The vortex line density of the tangle can easily be determined by measuring the attenuation of second sound across the channel, or temperature gradients down the channel, as discussed above. The TI–TII transition is most easily observed in narrow channels. Tough's group have reported complex dynamical features of this transition (Lorenson *et al* 1985), made by measuring the chemical potential difference $\Delta\mu$ across a short (1 cm), narrow glass tube (diameter 0.0134 cm). These measurements show that the vortex line density L_0 above critical is approximately proportional to the square of the driving counterflow velocity. At TII there is a dramatic increase in superfluid vortex density. This leads to the conjecture that the TI–TII transition is caused by some instability in the normal fluid: indeed, what is the effect of the tangle on the normal fluid itself? This question has been addressed by Melotte and Barenghi (1998). The authors considered the stability of the normal fluid under increasing forcing due to the tangle at ever increasing values of L_0 using standard linear stability theory. The results are quite dramatic as seen in figure 9. While the temperature dependence does not seem quite right (the detailed situation is probably more complicated than that considered by the authors), the fact that the magnitude is correct is really quite satisfying. The picture which emerges from the calculations is that in state TI the superfluid is turbulent, but the density L_0 of the superfluid vortex tangle is not sufficient to alter the laminar profile of the normal fluid. At sufficiently large counterflow velocities a transition takes place and the normal fluid velocity profile is destabilized. The linear theory cannot predict what will happen beyond critical, but a good guess is that the normal fluid becomes turbulent. The TII state therefore corresponds to turbulence in both superfluid and normal fluid components.

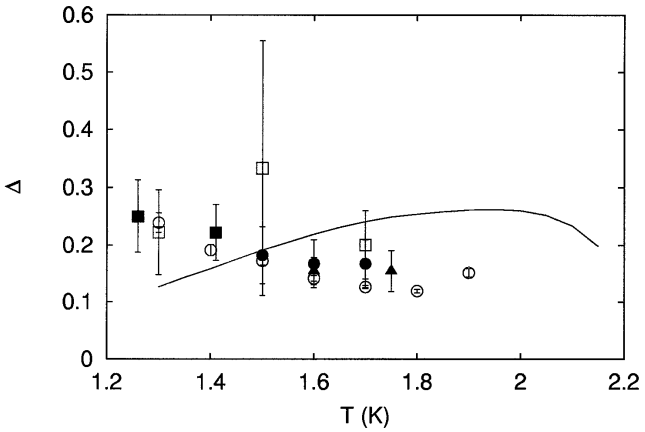

Figure 9. Transition between TI and TII states: comparison between theory and experiments. TI–TII transition, full curve (Melotte and Barenghi 1998). Various experiments are indicated by different symbols.

4.6. Simulations of counterflow turbulence

4.6.1. Methods of simulation. The dynamics of vortices in helium II forms a particularly attractive problem to simulate numerically. The equations of motion are well known and, because of the microscopic core size, a thin vortex filament approximation is very good. One needs to follow only a one-dimensional set of points moving in three-dimensional space, rather than a three-dimensional set as in, for example, simulations of the Navier–Stokes equation. In addition, Arms and Hama (1965) developed a simple local approximation to the vortex line induced velocity which is discussed briefly below. Despite this attractiveness, significant simulations of quantum turbulence have been carried out only by Schwarz (1978, 1982, 1983, 1985, 1988) at IBM over a number of years and more recently by Aarts and DeWaele (1994).

A useful generalization of the analytical vortex ring calculation in books such as Lamb was obtained by Arms and Hama (1965). Its importance lies in making possible approximate calculations of the motion of arbitrary configurations of very thin vortex lines. The fluid velocity at some point in space, induced by a vortex line, is given by an exact analogy in the theory of electromagnetism called the Biot–Savart law. In this analogy the fluid velocity corresponds to the magnetic field $\boldsymbol{H}$ and vorticity ω to the current density $\boldsymbol{j}$. The equation $\omega = \operatorname{curl} \boldsymbol{v}$ is analogous to Maxwell's equation $\operatorname{curl} \boldsymbol{H} = (4\pi/c)\boldsymbol{j}$. The integration is over all of the vortex singularities in the fluid boundary effects are included by extending the integral to the images of the singularities.

If an arbitrary segment of vortex line is parametrized as in figure 10, then the Biot–Savart law can be written as

$$\boldsymbol{v} = (\kappa/4\pi) \int (\boldsymbol{s}_0 - \boldsymbol{r}) \boldsymbol{\chi} \, \mathrm{d}\boldsymbol{s}_0 / |\boldsymbol{s} - \boldsymbol{r}|^3 \tag{4.58}$$

where $\boldsymbol{r}$ is any point in the fluid and the integral is over the relevant line segments. If $\boldsymbol{r} = \boldsymbol{s}_0$ is a point *on* the line, the integral in (4.58) diverges. If we expand $\boldsymbol{s}$ in a Taylor series about $\boldsymbol{s}_0$, $\boldsymbol{s} \approx \boldsymbol{s}_0 + \boldsymbol{s}'\xi + \frac{1}{2}\boldsymbol{s}''\xi^2$ and (4.58) becomes

$$\boldsymbol{v} \approx (\kappa/4\pi) \int (\mathrm{d}\xi/2\xi) \boldsymbol{s}' \times \boldsymbol{s}'' \tag{4.59}$$

where the integral is over the whole vortex array except for a distance of the order of the core radius a on either side of $\boldsymbol{s}_0$. Ignoring 'non-local' portions of the vortex (more than some

distance L away from s_0 measured along the arc) and approximating the cross-product by its value at s_0, we get the local self-induced velocity

$$v_i \approx (\kappa/4\pi)\ln(L/a)s' \times s'' \tag{4.60}$$

where $s' \times s''$ has the magnitude $1/R$, R being the radius of curvature at s_0.

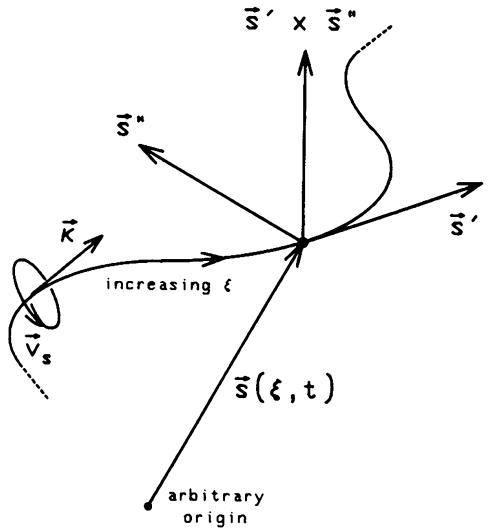

Figure 10. A drawing of the parametric notation use to describe a vortex line tangle. The curved line represents a vortex line with its position described as $s(\xi, t)$. The local tangent $s' = \hat{\kappa}$, where $\hat{\kappa}$ is a unit vector along the vortex line in the direction of κ, s'' is the local curvature vector (whose magnitude is $1/R$), and the binormal $s' \times s''$ is in the direction of the tangle-induced velocity v_i and also has the magnitude $1/R$. The instantaneous velocity of the line is given by $v_L = \mathrm{d}s(\xi, t) = \dot{s}$.

In scalar terms

$$v_i \approx (\kappa/4\pi)\ln(L/a). \tag{4.61}$$

The choice of L to best approximate (4.58) depends on the details of the vortex configuration.

If we wish to include the 'far field' of the vortex we can make a rough approximation by integrating (4.58) over the line omitting a region along the vortex of length L on either side of s_0. Then

$$v_{(non\text{-}local)} = (\kappa/4\pi)\int' (s_0 - r) \times \mathrm{d}s_0/|s - r|^3 \tag{4.62}$$

where the prime on the integral indicates that the local line element is omitted.

An immediate application of (4.61) is an intuitive understanding of how a vortex ring moves through a fluid: if L is replaced by R we have an approximation to (4.58). A vortex ring moves through the fluid principally because of its curvature. As an example a ring with $a = 10^{-8}$ cm and $R = 10^{-3}$ cm moves through the liquid at about 1 cm s^{-1}. A numerical simulation was carried out in our laboratory using a mesh of 100 points on the circumference. The localized induction, cut off at nearest neighbours from a selected origin, provided 73% of the total induced velocity.

4.6.2. Major insights from the simulations. Schwarz (1978) has shown that the Arms–Hama local induction approximation (hereafter referred to as the local approximation) is generally

valid in quantum turbulence, but that there are some instances when the 'far field' becomes important. These instances occur when previously distant portions of the tangle or the tangle and its image approach more closely than a critical distance (Schwarz 1985). Thus vortex simulations can be successfully broken down into two parts:

(i) a local approximation which is generally valid;
(ii) discrete events, line–line or line–boundary 'crossings', where the far field is significant.

With a local approximation, portions of the tangle with small radius of curvature or local induced velocity v_i opposite to the counterflow will evanesce due to mutual friction. Other portions will grow and be annihilated at the walls. Thus vortex crossings are necessary to keep a tangle self-sustaining, and the treatment of such crossings is crucial to a successful simulation. In early work, Schwarz (1978) forced a randomization of the vortex configuration in the vicinity of the crossing, which was costly in computer time, but allowed successful simulations of steady-state flows without boundaries.

A second major insight from Schwarz's work (Schwarz 1982) is that one can replace the configuration randomization with a simple 'topology-changing reconnection', with similar results and a great increase in ease of implementation. Such reconnections are depicted in figure 11. In recent work, Schwarz (1985) has shown that a reconnection is feasible, but classical vortex dynamics breaks down as the distance of closest approach becomes of the order of the core size, and one is left with a quantum mechanical problem. There is some evidence (Schwarz 1982) that, in fact, a topology changing reconnection does not occur at every crossing. What really happens at a crossing is a major unsolved problem in quantum turbulence.

Probably the greatest lesson from Schwarz's simulations is the success in reproducing phenomena which has been achieved using the equations of vortex dynamics with several simplifying assumptions. The counterflow was assumed to be uniform, as in state TIV (pure superflow), the velocity dependence of α and β (see equations (4.43) and (4.51)) was ignored (eliminating the weak velocity dependence of L_0/v_{ns}^2), α was ignored (valid except near T_λ), and periodic boundary conditions were used (ensuring homogeneity of the line density).

In early simulations (Schwarz 1978), i.e. prior to implementing the reconnection ansatz, boundaries were ignored and thus critical velocities were not reproduced. Nevertheless, the success was quite remarkable. The v_{ns}^2 dependence of L_0 was reproduced (as scaling arguments now show must happen). The mutual friction force and the line density were in surprising quantitative agreement with experiment, well within the range of the rather scattered experimental results of the time.

Implementation of the topology changing reconnection ansatz allowed boundaries to be included through line–boundary reconnections (although v_{ns} remained uniform). With this improvement, Schwarz (1983) was able to reproduce v_{c1} and v_{c3}, the first critical velocity in small- and large-aspect-ratio channels. It is curious that the temperature dependence of the critical velocity found by the simulations was much stronger than v_{c4} (Baehr and Tough 1985), and indeed similar to that in counterflow. Awschalom *et al* (1984) report new calculations of γ (smaller than those reported by Schwarz (1978)) which agree remarkably well with the measurements of γ_2 and with the most recent measurements of γ_4 (Opatowsky and Tough 1981).

4.6.3. Vortex reconnections, results of the simulations. The idea of vortex reconnections was first put forward by Feynman (1955) in his discussion of the decay of a vortex tangle into heat. When two oppositely-directed bits of vortex line approach closely enough, one might speculate that the reduction in the scale of the flow might cut off the circulation and hence allow the

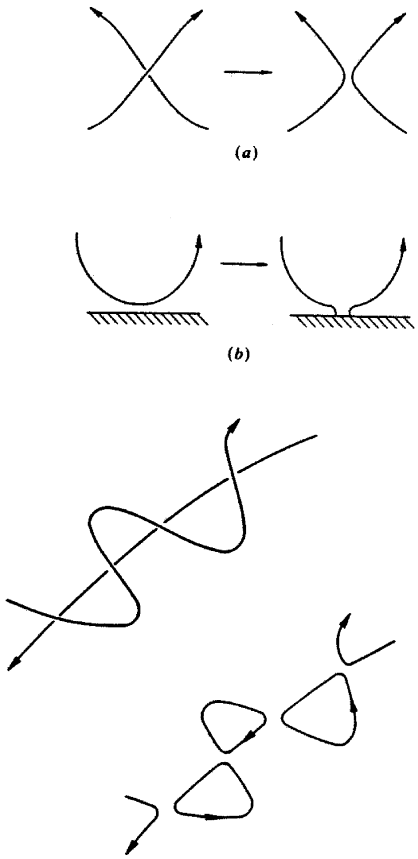

Figure 11. Illustration of (a) a possible reconnection sequence between vortex filaments in a tangle, (b) a vortex filament reconnection at a surface and (c) multiplication of singularities through the reconnection process. Here two vortex lines reconnect to form five. After Schwarz (1988).

reconnection process to occur without violation of Kelvin's circulation theorem. This problem has not been directly addressed, and is likely to be a difficult problem in quantum mechanics. Some indirect evidence, however, exists. Jones and Roberts (1982) have made a study of the Ginzburg–Pitaevskii equation for a family of vortex rings of steadily decreasing ratio of radius to core size. They find that at a definite value of this quantity, the circulation disappears, and the remnant of the vortex becomes solitary waves of compression. In the most recent paper on motions in a Bose condensate, Jones *et al* (1986) have demonstrated by direct numerical calculation the establishment of a vortex core and circulation in the evolution of the nonlinear Schrödinger equation.

The Schwarz simulation has gone beyond the Feynman speculation in addressing the problem of a self-sustaining tangle. In particular, he has shown that when bits of line approach which are parallel in sense of circulation, the line can wrap around in such a way as to allow reconnection to take place. The final resolution of the quantum mechanics is a challenging problem, but at the present time it looks as if the necessary conceptual basis is given by the Jones and Roberts calculation. The NLSE model has been used to demonstrate the existence of reconnections (Koplik 1993) which are postulated in the vortex dynamics approach of Schwarz.

The results of Schwarz's calculations are contained in his main paper on the subject (Schwarz 1988). One interesting example is shown in figure 12, where the friction constant

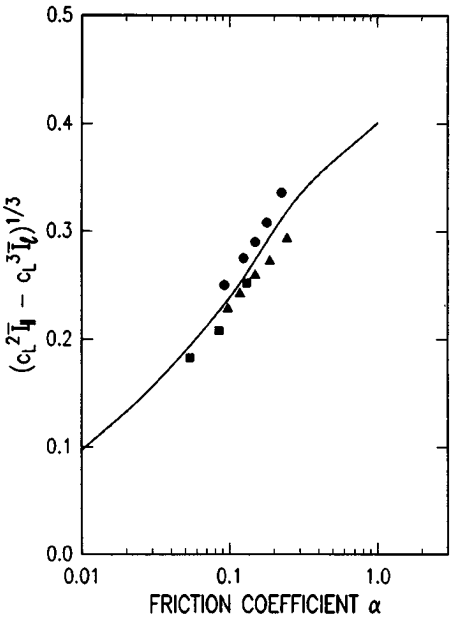

Figure 12. Comparison of the theoretically predicted mutual friction force coefficient with experiment. After Schwarz (1988).

$\alpha = B\rho_n/2\rho$ is varied, not by changing temperature as is usual, but by changing the pressure. Other examples of the success of the simulations are contained in figures 7 and 8.

There are many pictures of the vortex tangle in various publications. Probably the most interesting are again in the 1988 paper by Schwarz.

The total experience gained from vortex simulations has allowed Schwarz to give us a graphic picture of the way a tangle of vortex lines is sustained:

'The self-induced velocity causes a complicated three-dimensional internal motion of the vortex tangle, the whole thing being washed along by any applied superflow field v_s which may be present. Highly curved sections of line, and sections propagating opposite to v_{ns}, decay. Simultaneously, other parts of the vortex tangle where the self-induced motion is being overtaken by the v_{ns} field grow by ballooning outwards. The cross-steam nature of the vortex growth implies that in the steady state at least a certain fraction of the singularities is constantly being driven toward the walls. The line–line reconnections which occur as the vortex tangle undergoes its complicated dance play several important roles. First, they provide a mechanism by which new vortex singularities can be created (figure 11), allowing the vortex tangle to be established and sustained against the loss of singularities at the walls. Secondly, and more subtly, since the vortex amplification process is essentially a two-dimensional outward motion in the plane perpendicular to v_{ns}, the reconnections and the subsequent motions along v_{ns} which result are necessary to maintain the three-dimensional random nature of the vortex tangle. Finally, the reconnections occur more often as the tangle becomes denser. The increasing frictional line loss associated with the creation of a more and more highly curved vortex tangle is the factor which eventually limits the tangle density. All of these complicated dynamical features interact self-consistently to produce the turbulent steady state.'

4.6.4. Self-consistent turbulence. The drawback of Schwarz's vortex dynamics approach is that it is essentially *kinematic* in character: the driving fields v_n and v_s are imposed at the

beginning of the numerical calculation and never change. This limitation is present in all work published until recently. For example, when studying counterflow turbulence, Schwarz set $v_n - v_s$ equal to a constant, proportional to the driving heat flux. Choices of v_n used in the literature range from uniform flows in periodic boxes or channels, Poiseuille flows, a single vortex tube and Arnold–Baltrami–Childress (ABC) flows. In each case the shape of the profile of v_n was fixed.

The difficulty of kinematic models becomes apparent, when viscous flows of the normal fluid with boundaries are studied, such as channel flows. On one hand, it can be argued that v_n should have a parabolic Poiseuille profile to satisfy the no-slip boundary conditions at the wall; on the other hand, one can also argue that the parabolic profile becomes so flattened by the friction with the superfluid vortex tangle that a uniform profile may be a better choice. Aarts and DeWaele (1994) tested both these profiles and, not too surprisingly, they found that the vortex tangle looks very different if v_n is parabolic rather than uniform.

The same difficulty appears when one tries to determine the normal fluid flow as a function of a fixed tangle rather than *vice versa*. This was attempted by Melotte and Barenghi (1998) as described in section 4.5.13, who studied the linear stability of v_n under the forcing of an imposed homogeneous and isotropic vortex tangle. Their calculation showed that if the vortex tangle exceeds a critical density the Poiseuille profile becomes unstable and possibly turbulent, a transition which would clearly change the vortex tangle itself.

In a recent paper Barenghi and Samuels (1999) showed how to overcome the difficulty of the kinematic approach. They proposed a new, dynamically *self-consistent* approach, which takes into account the back-reaction of the vortex tangle onto the normal fluid. The idea consists in letting the normal fluid evolve alongside the tangle of superfluid vortex lines, according to its own equation of motion. In this way the vortex tangle and the normal fluid profile determine each other in a dynamically self-consistent fashion. For example, in the channel flow problem studied by Aarts and DeWaele, the calculation would start as usual with few superfluid vortex lines to act as seed, while the normal fluid would be initially in the correct parabolic profile to satisfy the boundary conditions; as the vortex tangle develops, the back reaction of the tangle onto v_n via friction would increase, changing the parabolic profile of v_n. In this way, if the friction is large enough, v_n may become distorted, flattened or even turbulent, as argued by Melotte and Barenghi (1998) in the context of heat transfer flow.

To implement the new approach they considered the equation of the normal fluid, which they assumed isothermal and incompressible for simplicity. Neglecting any externally applied superfluid potential flow, this equation is the Navier–Stokes equation modified by the introduction of the friction force,

$$\rho_n \frac{\partial \boldsymbol{v}_n}{\partial t} + \rho_n (\boldsymbol{v}_n \cdot \nabla)\boldsymbol{v}_n = -\frac{\rho_n}{\rho}\nabla P + \eta \nabla^2 \boldsymbol{v}_n + \boldsymbol{F}_{ns} \tag{4.63}$$

where P is the pressure. Equation (4.63) must be solved together with the continuity equation $\nabla \cdot v_n = 0$. The friction force per unit volume at a given point is

$$\boldsymbol{F}_{ns} = \frac{\kappa B \rho_n \rho_s}{2\rho} \frac{1}{V} \int \boldsymbol{s}' \times [\boldsymbol{s}' \times (\boldsymbol{v}_n - \boldsymbol{v}_s - \boldsymbol{v}_i)]\, \mathrm{d}\xi \tag{4.64}$$

where the integration is performed over the vortex lines in the volume V around that particular point. Note that until now the calculation of the friction has been attempted for diagnostic reasons only, in the context of kinematic models.

The self-consistent approach consists therefore in determining the evolution of the vortex tangle for a given v_n (as done by Schwarz), while at the same time determining v_n from (4.63) and (4.64).

Barenghi and Samuels (1999) implemented this new approach in a calculation of the decay of a model of normal fluid eddy coupled to a decaying vortex tangle. Their calculation was rather idealized because it was performed in a periodic box of size λ (like the ABC flow calculation of Barenghi *et al* (1997)) and the normal fluid was only two-dimensional. Barenghi and Samuels found that after an eventual initial rise (which depends on the relative energies contained in the normal fluid and superfluid initial condition) the energy of the normal fluid eddy decays with the behaviour $e^{-\sigma \hat{t}}$ independently of temperature, where $\hat{t}$ is time scaled with the kinematic viscosity of the total helium density $\nu = \eta/\rho$ rather than $\nu_n = \eta/\rho_n$. This uniform value of the decay constant is at first surprising: how does the normal fluid know about the *total* helium density? Note that the temperature range covered by the results corresponds to a normal fluid fraction ρ_n/ρ which varies between 99% at $T = 2.171$ K to only 56% at $T = 2.0$ K. In the absence of a tangle the energy of the normal ABC flow should decay exponentially with time scale based on ν_n.

The interpretation of the data is that the coupling between the normal fluid and the tangle is strong enough to compensate for the changing relative proportion of normal fluid. Although the model is too idealized to make a direct quantitative comparison with the experiments, the result is consistent with the observation by Stalp (1998) that the decay rate of helium turbulence is independent of temperature (see section 4.8.2).

4.7. Co-flows and vortex coupled superfluidity

4.7.1. Periodic boundary layer experiments. The damping of oscillating disks in liquid helium was originally studied in the 1930s in order to determine the viscosity. After World War II, experiments by Andronikashvili (1946), Hollis Hallet (1955), Benson and Hollis Hallett (1956) and Donnelly and Penrose (1956) have shown that oscillation experiments can also be used to study the hydrodynamics of helium II.

The damping of oscillations in helium II may be conveniently discussed in three different ranges of amplitude. At low amplitudes the experimental data are consistent with a linearized set of two-fluid equations which neglect the effect of mutual friction. At higher amplitudes the normal and superfluid components move together and the results are consistent with a single equation, the Navier–Stokes equation. There is sometimes a quite sudden rise in damping observed between these amplitude ranges which corresponds not to a large change in the viscosity of the liquid, but to a radical change in the hydrodynamic flow pattern. At the highest amplitudes turbulence is observed in both helium I and helium II.

In the case in which the normal and superfluid components move together a kinematic viscosity can be defined representing the ratio of the viscosity to the total density of the liquid. These experiments were the first to show convincingly that the two fluid equations of motion for helium II are not applicable to flows with suitably defined Reynolds numbers greater than order 100. Indeed these experiments raise the question as to whether helium II might be used as a means to study classical turbulence.

The transition to 'turbulence' shown in figure 13 is probably not really turbulence in the accepted sense. In particular, for the oscillating sphere, a stability theory by Otto (1992) has now appeared. A preliminary phase diagram has been established showing an appropriately defined Taylor number versus R/δ, where R is the radius of the sphere and δ the viscous penetration depth. The onset of instability against Taylor vortices in an unpublished experiment in water agrees reasonably with the theory of Otto, and shows that the first departure from stability is the formation of Taylor vortices at the equator. Thus we are gaining an understanding of periodic boundary layer experiments in ordinary fluids and perhaps can soon return to the explanation of the first critical velocity.

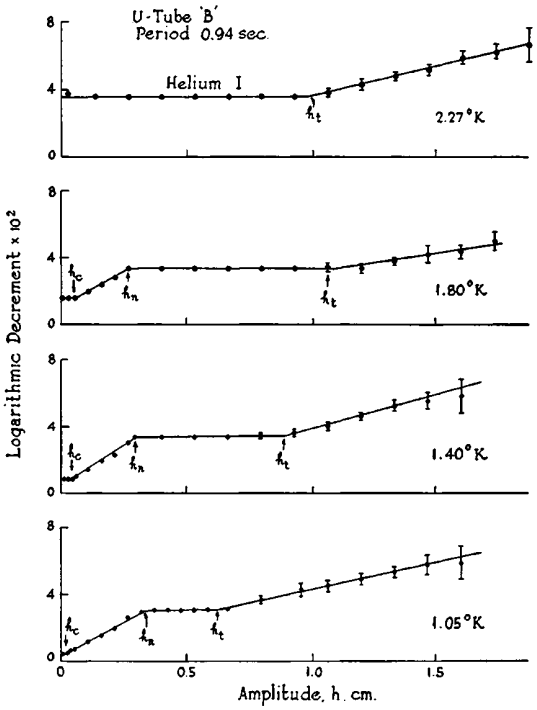

Figure 13. The variation with amplitude of the damping of gravity oscillations of liquid helium in a U-tube at a period of 0.94 s. After Donnelly and Hollis Hallett (1958).

4.7.2. Vortex coupled superfluidity. Because the flow of helium II is described by the two-fluid model, it is certainly not, at first sight, a conventional Navier–Stokes fluid. It is not clear that turbulence in helium II should behave as does classical turbulence. For instance, as discussed in section 4.5 above, when heat is applied at the end of a closed channel a counterflow turbulent state can be generated which is not achievable in classical flows. In a number of isothermal situations, such as the periodic boundary layer experiments discussed above, it is found experimentally that the two fluids couple together behaving in many ways like a classical Navier–Stokes fluid (Donnelly 1991a, b). This coupling of the fluids which we refer to as *vortex-coupled superfluidity* is the subject of the rest of this section. It is important to note that we are not referring to a perfect coupling. Such is clearly impossible since the normal fluid is thought of as having continuously distributed vorticity, while the superfluid has discrete quantized vortices. Instead we envision a coupling length scale l_c larger than the distance between the lines, l, but smaller than other physically relevant length scales λ, that is $l < l_c < \lambda$. Evidence for the coupling is found in both experiment and scaling arguments.

Early experiments which revealed the classical behaviour of helium II at high Reynolds number studied the drag coefficient of a sphere: Dowley *et al* (1961) and Laing and Rorschach (1961). It was found that the drag coefficient is not markedly different in helium I than in helium II. More recently, experiments have examined both pump performance and pressure drops in flow through smooth and rough pipes using helium II (Walstrom *et al* 1988). The pressure drops scale well with the classical results, from which we infer that the velocity profiles also scale, namely that a thin viscous sub-layer which generates the pressure drop forms near the wall. The pump performance in helium II is also identical to that in helium I.

In Taylor–Couette flow Bielert and Stamm (1994) investigated high Reynolds numbers ($Re \sim 40\ Re_c$). They used a method of flow visualization in helium based on small tracing particles by which they could examine pattern formation. They saw that in this turbulent regime the Taylor rolls have wavelength approximately equal to the gap's size, which is identical to the classical case.

4.7.3. Decay of superfluid turbulence. Evidence on coupled flows can also be found in experiments on vortex decay. Schwarz and Rozen (1991) have investigated the decay of *superfluid* vorticity generated by counterflow. In counterflow turbulence, a very large superfluid vorticity is generated due to the relative velocities between the two fluids. The normal fluid vorticity, however, is much less robust. The initial decay of the superfluid vorticity is well described by vortex-tangle theory (section 4.5.2), but this initial period is followed by a period of slower decay not obeying the expected scaling laws. The slow decay is interpreted by Schwarz and Rozen as follows: 'The superfluid vorticity decays to a level equal to the normal fluid vorticity. The normal fluid vorticity meanwhile is decaying slowly through viscous dissipation in accordance with classical turbulent scaling laws. Instead of decaying to zero, the superfluid vorticity is maintained by eddies in the normal fluid. The normal fluid vorticity maintains the superfluid vorticity, and thus the fluids are coupled.'

Another hint is contained in section 4.8.3 where there is some experimental evidence that, at long times, the counterflow-created turbulence decays like a classical fluid.

4.7.4. Turbulent flow over a sphere. One characteristic of classical turbulent flow is evidenced by the celebrated relationship between drag coefficient and Reynolds number for flow about a sphere. At a Reynolds number of about 10^5 there is a sudden fall in the drag coefficient which has been known for decades. The question of whether that fall exists in helium I and helium II was first taken up by Laing and Rorschach (1961) with somewhat inconclusive results. Recently Smith *et al* (1999) have built an apparatus which establishes the drag on the sphere by direct measurement of the pressure distribution as shown in figure 14. The distributions of pressure are shown in figure 15 in helium II and results in helium I are very similar. The drag coefficient as a function of Reynolds number is shown in figure 16 and clearly indicate the drag crisis is present in both helium I and helium II. This is a first report on an ongoing study which will extend measurements in both Reynolds number range and temperature in helium II.

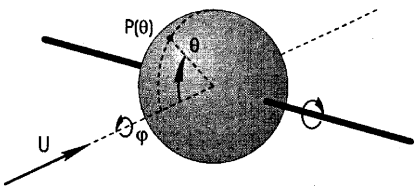

Figure 14. Pressure distribution device designed by Smith *et al* (1999). A single pressure tap is used to map out the pressure profile over the meridian shown by the dashed line on the sphere. The pressure signal is sent to a sensor through one of the support struts.

4.7.5. Vortex tubes. A key observation to model turbulent helium II was first made by Samuels (1992) that the presence of normal fluid vorticity has a significant effect on superfluid vortex lines. In most experiments under consideration the Reynolds number is high and the normal fluid must be turbulent. It is known from the observations and from the numerical simulations

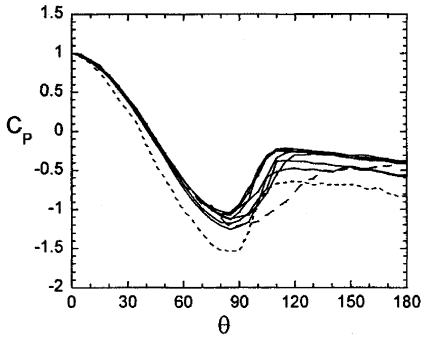

Figure 15. Pressure distribution for various Reynolds numbers at 1.8 K in helium II. The long and short dashed curves correspond to $Re = 1.1 \times 10^5$ and 1.3×10^5, respectively. Others range from $Re = 1.7 \times 10^5$ to 9.6×10^5. The situation in helium I is much the same. After Smith *et al* (1999).

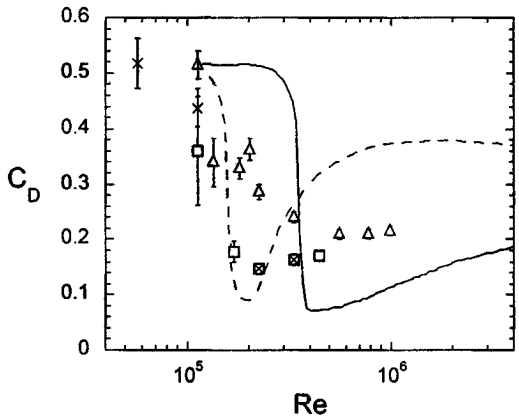

Figure 16. Drag coefficient as a function of Reynolds number. The open squares and crosses correspond to temperatures 2.54 K and 4.2 K, respectively. The triangles were recorded at 1.8 K. The full curve is the accepted classical result and the dashed curve shows the effect of a surface roughness of 0.0015. After Smith *et al* (1999).

of classical turbulence (for example, She *et al* 1990) that regions of intense concentrated vorticity appear in the flow, move about and disappear after a certain time. We expect that the normal fluid has similar regions of concentrated vorticity. To model these vortex tubes, Barenghi *et al* (1997) chose an ABC flow. Using Cartesian coordinates (x, y, z) the normal fluid velocity v_n has components given by

$$\begin{aligned} u_n &= A\sin(2\pi z/\lambda) + C\cos(2\pi y/\lambda) \\ v_n &= B\sin(2\pi x/\lambda) + A\cos(2\pi z/\lambda) \\ w_n &= C\sin(2\pi y/\lambda) + B\cos(2\pi x/\lambda) \end{aligned} \tag{4.65}$$

where λ is a length scale and A, B and C are parameters. ABC flows are solutions of the steady Euler equation and of the time-dependent, forced Navier–Stokes equation. Despite the apparent simplicity, the streamlines have a complex Lagrangian pattern which includes a chaotic particle path at certain values of parameters (Dombre *et al* 1986). ABC flows have also been used to study turbulent processes of dynamo action in magneto-hydrodynamics (Gilbert *et al* 1993, Galloway and Proctor 1992). Finally, ABC flows have non-zero helicity, a property which

has been associated with turbulence structures both in experiments and numerical simulation (Moffat and Tsinobar 1992).

The numerical simulation calculated the time evolution of an arbitrary initial superfluid vortex configuration in the presence of a driving normal ABC flow. The calculation was performed inside a three-dimensional periodic box of size λ. Typically the calculation started with an initial superfluid vortex ring. Under the influence of the normal flow, the ring became unstable and distorted, the total length of the vortex line increased and a vortex tangle developed, as showed in the time sequence of figure 17.

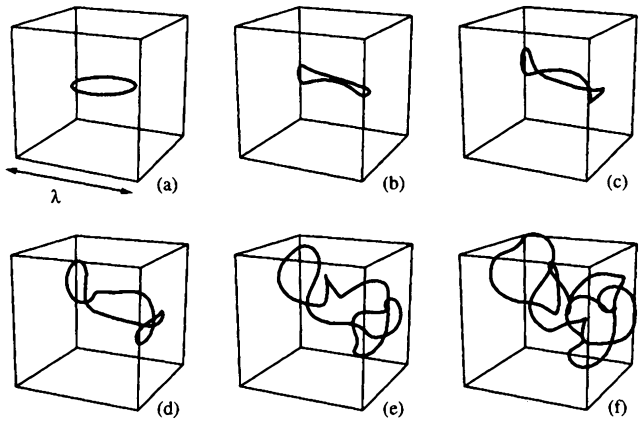

Figure 17. Time evolution of a single vortex ring in a normal fluid ABC flow. The calculation is performed in an infinite volume, without using periodic boundary conditions.

The physical mechanism underlying this process is the instability of a superfluid vortex line to the growth of helical vortex waves (Kelvin waves), which is illustrated in figure 18.

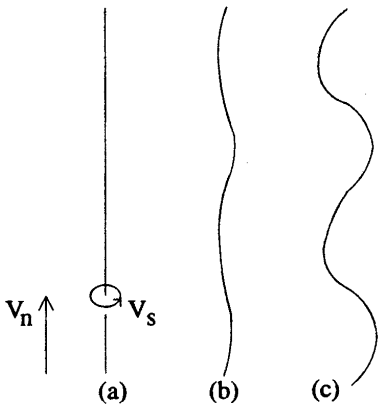

Figure 18. The Donnelly–Glaberson instability of a quantized vortex line which occurs if a normal fluid flow has a component parallel to the core of the line.

The instability occurs if the component of the normal fluid velocity in the direction parallel to the vortex line exceeds a critical value, as discovered by the Donnelly group and explained by the Glaberson group (Cheng *et al* 1973, Ostermeier and Glaberson 1975). As vortex waves become unstable and grow, more line length is created, hence more vortex line length

undergoes the same instability, and so on, until nonlinear effects saturate the growth. Barenghi *et al* noticed that the instability generates bundles of superfluid vortex lines which, driven by mutual friction, concentrate in the regions where the vorticity of the ABC normal fluid is high, see figure 19.

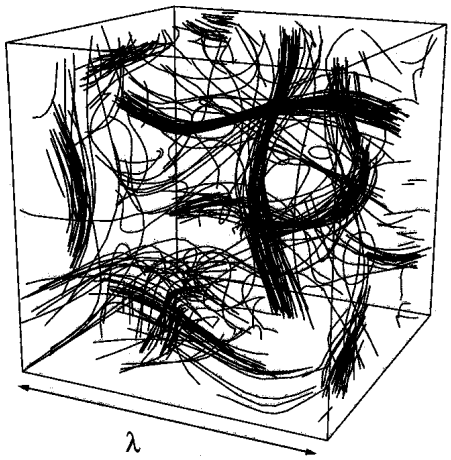

Figure 19. A more organized vortex tangle arising from operation of the vortex line instability. This calculation is done in a periodic box. After Barenghi *et al* (1997).

Although the *microscopic* superfluid velocity pattern in the bundles is very complicated, its *macroscopic* average ω_s over a region larger than the intervortex separation is similar to the vorticity field ω_n of the normal fluid. This *vorticity matching* is consistent with the observations. Numerical investigation of the growth time scale for the vortex lines showed that it is of the same order of the ABC flow time scale; since the lifetime of the vortex tubes observed in turbulence is of the order of few turnover times, there is enough time for the matching process to take place.

Although the ABC model is too simple to make direct quantitative comparison with the experiments, it confirms the locking mechanism which has been postulated to explain the experiments and provides a physical explanation for this mechanism.

4.7.6. A damping length scale for superfluid turbulence. Samuels and Kivotides, in a recent preprint, have proposed that a damping length scale ℓ_{sd} can be defined for superfluid turbulence at non-zero temperatures, where the superfluid is coupled by mutual friction to the viscous normal fluid. Superfluid vortex structures (waves or rings) at length scales smaller than ℓ_{sd} will lose energy to the normal fluid and will be dissipated. They derive the Reynolds number dependence of this dissipation length scale and discuss the consequences of this length scale for the possible existence of a Kolmogorov $-5/3$ power law for the superfluid excitation spectrum.

From the Donnelly–Glaberson instability the authors define a length scale

$$\ell_{sd} = \frac{\kappa}{2V_{n,typ}} \ln\left(\frac{\ell_{sd}}{2\pi a}\right) \tag{4.66}$$

where κ is the quantum of circulation, $V_{n,typ}$ is some typical large velocity scale of the normal fluid and a is the superfluid vortex core radius. Superfluid vortex structures at length scales smaller than ℓ_{sd} will lose energy irreversibly to the normal fluid (where the energy will be dissipated to heat). Thus this length scale acts as a damping length scale

for the superfluid turbulence and simulations suggest it corresponds to the smallest radii of curvature in the superfluid vortex tangle. For a wide range of normal fluid Reynolds numbers ($100 < Re < 10^{11}$) the length scale ℓ_{sd} is within a factor of 10 of the normal fluid Kolmogorov length η. They discuss conditions under which the existence of this dissipation length scale for the superfluid leads to a Kolmogorov $-5/3$ energy spectrum. This $-5/3$ law would occur *without* the need for velocity matching between the superfluid and normal fluid.

4.8. Towed grid turbulence

4.8.1. The towed grid technique. The decay of homogeneous and isotropic turbulence (HIT) is regarded as one of the fundamental problems of fluid dynamics. Experiments on HIT are usually performed in wind tunnels that study grid-generated turbulence as it decays downstream (Batchelor 1953). A novel technique where turbulence is created by towing a grid through a stationary sample of helium II was first reported in Smith *et al* (1993). The authors analysed the decaying root-mean-square superfluid vorticity over a time span from 1 s to 5 s, where the energy containing length scale was assumed constant.

This technique has been improved in several ways in the past few years, allowing measurement of the rms superfluid vorticity over the range of $\sim 10^5$ to ~ 1 Hz. The apparatus is illustrated in figure 20. We define the superfluid vorticity as $\omega(t) = \kappa L$, where κ is the quantum of circulation and L is the length of quantized vortex line per unit volume obtained from measurement of the attenuation of second sound using a newly developed model suitable for arbitrary levels of attenuation (Stalp 1998). This definition is not free of problems and is still a matter of current research

Stalp (1998) has achieved mesh Reynolds numbers as high as 10^5 by towing a grid (mesh size $M = 0.167$ cm), with grid towing velocity (5 cm s^{-1} $< V_g <$ 200 cm s^{-1}), in a $1 \times 1 \times 56$ cm^3 channel. Observation of the turbulent decay over three orders of magnitude in time is equivalent to over 10^4 mesh lengths down a classical wind tunnel, making this system unique in the study of turbulence.

4.8.2. Decay of turbulence behind a towed grid. As explained in section 4.7.2 above, the normal fluid vorticity is assumed comparable to the observed vorticity of the superfluid, and the effective density is equal to the total fluid density ρ. In accord with this expectation, Stalp (1998) observed no appreciable difference in turbulent decays obtained over a temperature range of 1.4 K $< T <$ 2.15 K, which corresponds to an order of magnitude difference in the normal density ratio ρ_n/ρ. The decay is therefore analysed in terms of classical HIT. A model which attempts to describe the decay is presented in Stalp *et al* (1999). The essence of their model is shown in the assumed energy spectrum shown in figure 21. It is generally accepted that for small wavenumbers the total turbulent energy spectrum is of the form $E(k) = Ak^m$; with the usual choice $m = 2$. For large wavenumbers they use Kolmogorov's prediction $E(k) = C\varepsilon^{2/3}k^{-5/3}$, where C is the (dimensionless) Kolmogorov constant of order unity and $\varepsilon = -\mathrm{d}E/\mathrm{d}t$. These two wavenumber regions meet at $k_e(t) = 2\pi/l_e(t)$, where this peak in the energy spectrum corresponds to the energy containing eddy length scale $l_e(t)$, around which most of the turbulent energy resides. At large k, the spectrum is truncated at the Kolmogorov wavenumber k_η due to viscous dissipation. A novel aspect of their model is that at small wavenumbers the spectrum is truncated at $k_c = 2\pi/d$ owing to the size of the container. The energy-containing length scale grows until it saturates at the size of the container at time $t = t_s$ as shown in figure 21. These assumptions allow a straightforward analysis to be developed giving the form of the vorticity decay for all times as shown by the dashed curves in figure 22.

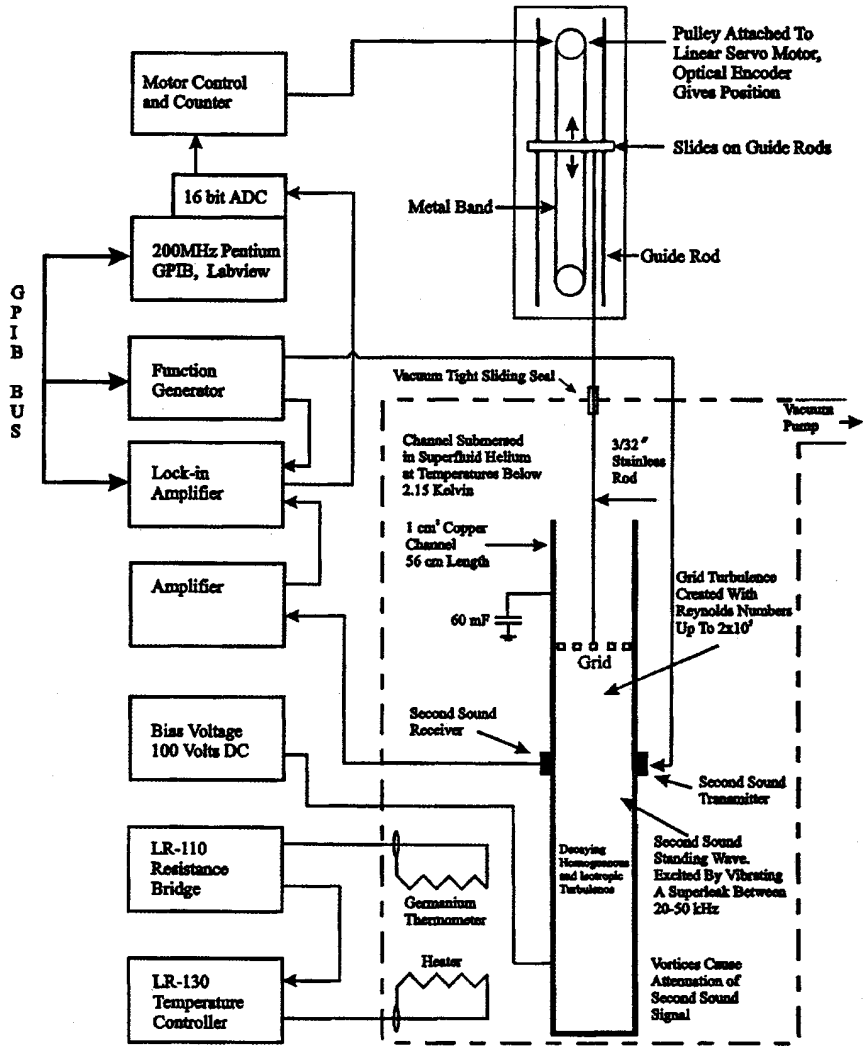

Figure 20. Schematic of experimental apparatus for towed grid experiments. An earlier version of this apparatus had provision to put a heater at the bottom of the channel to induce counterflow turbulence.

Typical experimental data taken at $T = 1.5$ K, for grid velocities of 5, 10, 50, 100 and 200 cm s^{-1}, are shown as full curves in figure 22. The plotted vorticity represents the rms superfluid vorticity averaged across the detecting volume of about 1 cm^3. At time $t = 0$ the grid passes a predetermined reference position located 7 mm above the middle of the detecting volume. The arbitrary reference position introduces a grid-velocity-dependent virtual origin that slightly affects the decay slope for times $t \ll t_s$. The individual decay curves possess a pronounced feature (see the arrows in figure 22) which is defined as the saturation time, t_s, so that the vorticity begins to decay as $\omega(t) \propto t^{-3/2}$. The authors believe this corresponds to the saturation of the energy-containing length scale at the size of the channel. They do not observe any appreciable departure from the asymptotic decay $\omega(t) \propto t^{-3/2}$ down to the level of a few hertz. The model leads to an experimental value of the three-dimensional Kolmogorov

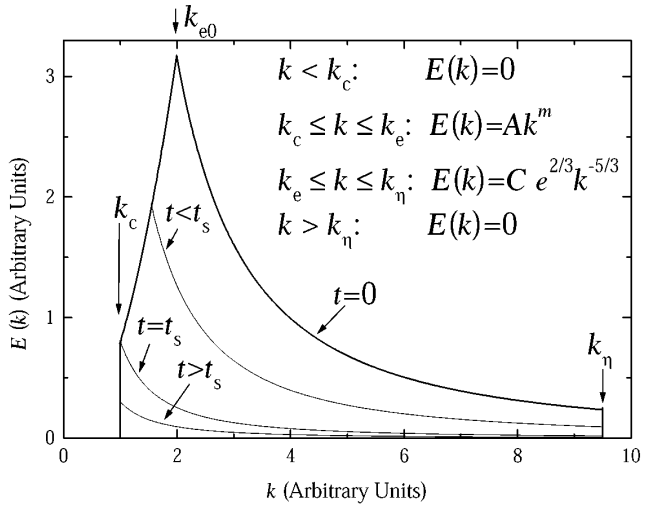

Figure 21. Schematic energy spectrum in developed HIT in a finite channel. After Stalp *et al* (1999).

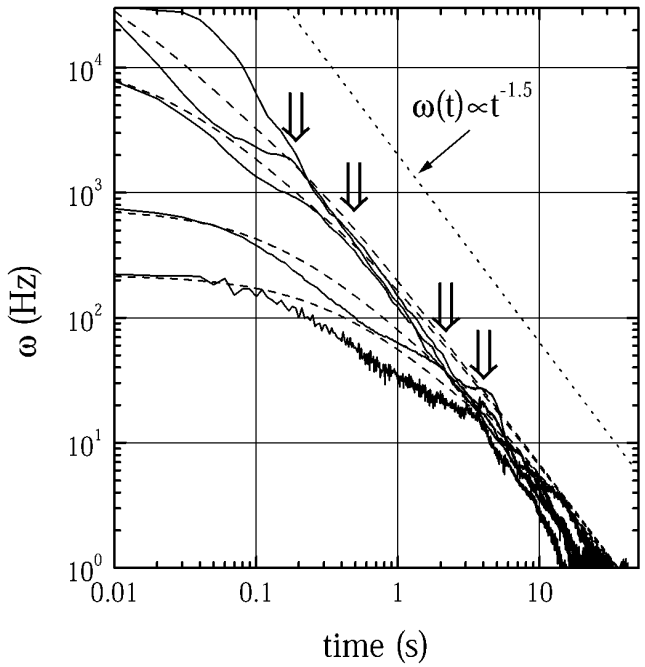

Figure 22. Decay of vorticity for grid velocities of 5, 10, 50, 100 and 200 cm s^{-1} (top solid curve) at 1.5 K. Dashed curves are from the model. The arrows indicate the time the energy-containing eddies reach the size of the container. After Stalp *et al* (1999).

constant $C = 1.3 \pm 0.2$. The fact that the experimental decay curves coincide at sufficiently long times demonstrates the independence of C from Re_λ (the Taylor microscale Reynolds number as defined below).

Values of these parameters of the model are derived for each grid velocity and the dashed

curves in figure 22 represent the associated theoretical decay curves calculated from the model. The results show that the initial energy containing length scale, l_{e0}, is typically only a few times smaller than the size of the channel.

The microscale Reynolds number is calculated as $Re_\lambda = \sqrt{15} l_e^{2/3} \nu^{-1/3} \omega^{1/3}$ (Stalp 1998). A vorticity of 1 Hz corresponds to $Re_\lambda \approx 85$. No appreciable variation in C over a wide range of Re_λ confirms that the Kolmogorov constant is independent of Re_λ and extends the Re_λ range from about 550 to over 10^3.

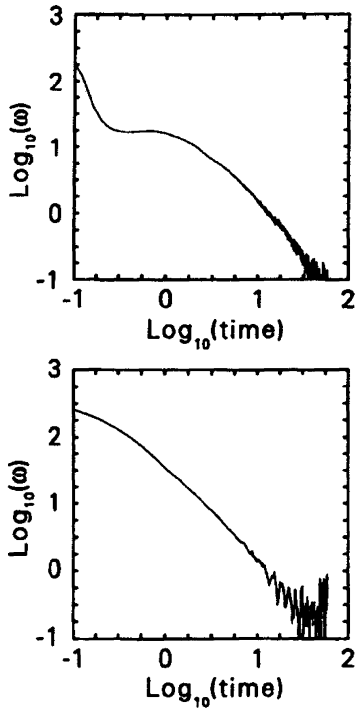

Figure 23. An illustration of the dramatic differences in decay of two turbulent flows of the same initial vorticity produced by a counterflow (upper curve) and towed grid (lower curve). The experimental channel was identical in both cases except the grid was removed for the counterflow experiment. The form of the upper curve has been discussed by Schwarz and Rozen (1991) and by Smith (1992). The decay curves coincide at long times and correspond exactly to the decay of classical turbulence.

4.8.3. Comparison between towed grid and counterflow turbulence. It is interesting to compare the turbulence created by counterflow in helium II and turbulence created by a towed grid in helium II (see figure 23). Simulations tell us that there are really only three scales in the counterflow experiment: the vortex core diameter, the average interline spacing and the size of the channel. There is no evidence of a cascade in the steady state. On the other hand, there is ample evidence of a cascade in towed grid turbulence, and that cascade persists throughout most of the decay period. It is interesting that at short times the decay of counterflow turbulence is radically different than towed grid turbulence. At long times the counterflow turbulence decay is seen to coincide exactly with the decay of towed grid turbulence starting from the same initial vorticity. It may be, then, that after some time, decaying counterflow turbulence tends to create a vortex cascade.

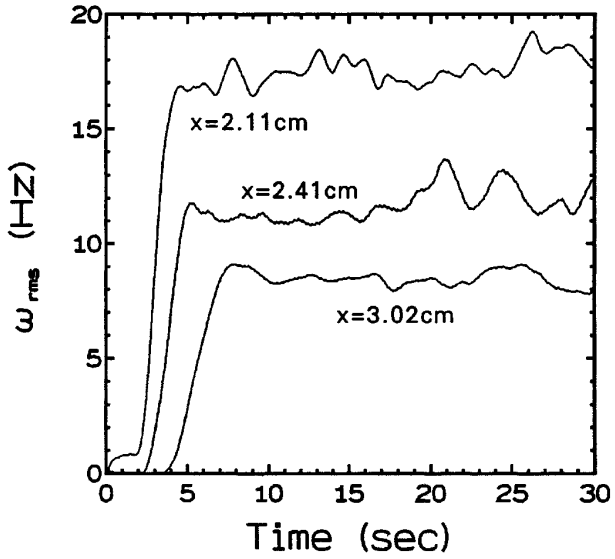

Figure 24. Typical averaged signal for the oscillating grid. The three values of x illustrate the effect of varying x on arrival time and steady state ω_{rms}.

4.9. Oscillating grid turbulence

There has been a good deal of interest in the turbulence generated by an oscillating grid either in water or in a stratified fluid. In an influential paper, Dickinson and Long (1978) make a strong case for a turbulent front propagating continuously and covering a distance proportional to the square root of the elapsed time using an oscillating grid in a water tank. We set out to investigate this motion in helium II and subsequently performed a number of qualitative experiments in water. The helium II investigations were carried out by Smith (1992) and form part of his thesis, the results in water are as yet unpublished.

The experimental protocol was to place the grid initially at some distance x from the detector, and at time $t = 0$ begin driving the grid up and down. The arrival time of the turbulent front was measured as a function of the stroke peak-to-peak amplitude $2a$, frequency f and distance x.

A triangular waveform for the oscillations was selected since the stepper motor control restricted us to this waveform for technical reasons. Subsequent water experiments used a four-bar linkage to produce a sinusoidal motion.

A typical averaged signal in helium II is illustrated in figure 24 for three different values of x. The sharp leading edge suggests a well defined front, certainly not diffusive in appearance. Smith was able to extract two quantities from his data: the arrival time of the front and the steady-state vorticity.

Figure 25(a) plots the arrival of the disturbance against x in the form $t^{0.435}$ versus x, for an oscillating frequency and stroke of 3.75 Hz and 2.5 cm, respectively. This best fit to the data was determined as before, although the method here was particularly insensitive to smaller exponents. This is illustrated by the plot of $t^{0.333}$ versus x shown in figure 25(b), which appears much the same as that of figure 25(a). These results then are far from conclusive. Moreover, other difficulties have arisen as we shall see next.

Finally, Smith measured the steady-state vorticity plotted in figure 26 as a function of distance away from the oscillating grid. The results suggest that the front does not propagate

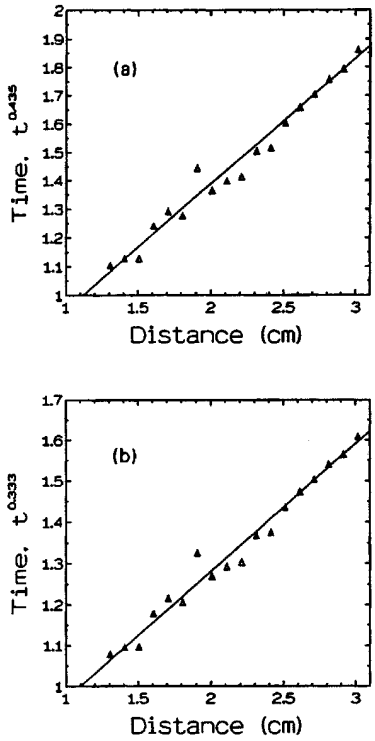

Figure 25. Position versus averaged arrival time for the oscillating grid. The best fit shown in (a) corresponds to $x \sim t^{0.435}$, but (b) clearly indicates that $x \sim t^{0.333}$ behaviour cannot be ruled out.

further than about 5 cm. This interesting result is in contradiction to the diffusive propagation of turbulence and motivated us to build an oscillating grid apparatus in water (Hall *et al* 1999). The water tank was constructed of Lucite and is 4 feet tall. Its cross section is square, 22 cm on side. The grid was driven by a stepping motor and four-bar linkage so a to obtain a sinusoidal stroke. While the details will be reported elsewhere, we found that the turbulent front does not propagate down the entire tank, but stops at a depth of the order of the width of the tank. Indeed, various diameter tubes were inserted in the tank, and the depth of propagation was observed as a function of the tube size. These very preliminary results suggest that the oscillating grid experiments do not follow the predictions of Dickinson and Long, and that such experiments form a rich subject matter which merits careful study in the future.

4.10. The Barenblatt burst

Barenblatt (1983) considered the behaviour of a turbulent layer initially confined to a region between planes at $x = \pm a$ as shown in figure 27. Barenblatt predicted that $h(t) = x(t) - a$, the distance from the initial front, should be given by

$$h(t) =\sim Q^{1/3}t^{2/3} \tag{4.67}$$

where Q is the energy contained in the burst at $t = 0$,

$$Q = \int_{-a}^{a} q(x, o)\,\mathrm{d}x \tag{4.68}$$

where $q(x, t)$ is the mean kinetic energy density of the flow per unit mass.

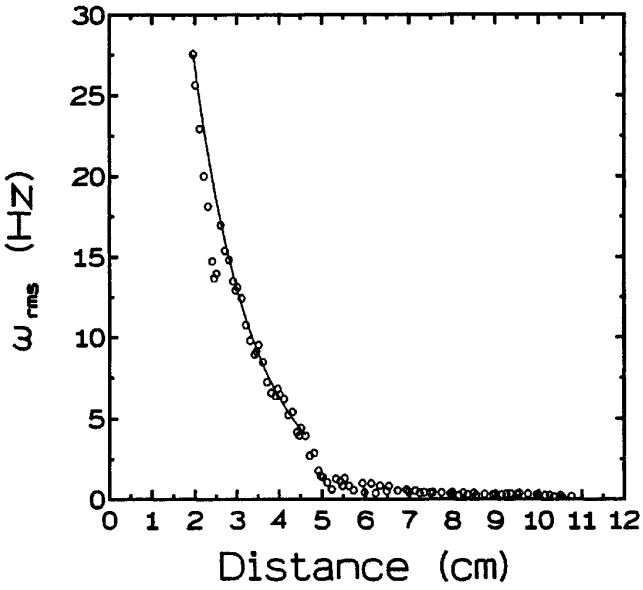

Figure 26. Steady-state vorticity for the oscillating grid in helium II as a function of distance (Smith 1992). We see that the turbulent front does not travel beyond about 5 cm. This behaviour is also seen in our unpublished oscillating grid water experiments, where the front propagates down the tank for a finite distance and stops.

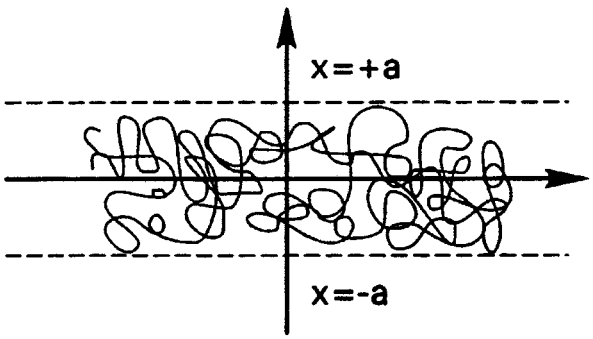

Figure 27. Barenblatt's problem: at $t = 0$ turbulence is confined to a layer extending from $x = -a$ to $x = a$. After a time t the fronts have propagated a distance $h(t)$ from the initial location of the layer.

Michael Smith has investigated this problem at Oregon in helium II by positioning the grid at various distances h above one of the second sound transducer pairs as shown in figure 20. At $t = 0$ the grid is pulled upwards to the top of the channel at velocities V, typically from 20 to 100 cm s^{-1}. In this way he created experimentally a layer of turbulence extending from the initial position of the grid to the top of the channel. Smith further assumed that this creates a single, sharp turbulent boundary, which will then spread downward to the collector below. He did indeed observe a distinct pulse arriving at the collector, which is shown in figure 28. The foot and peak of this pulse appear to travel together, although there is quite a spread in arrival times, forcing a reliance on large numbers of runs for good statistics. The cause of the spread is not yet understood.

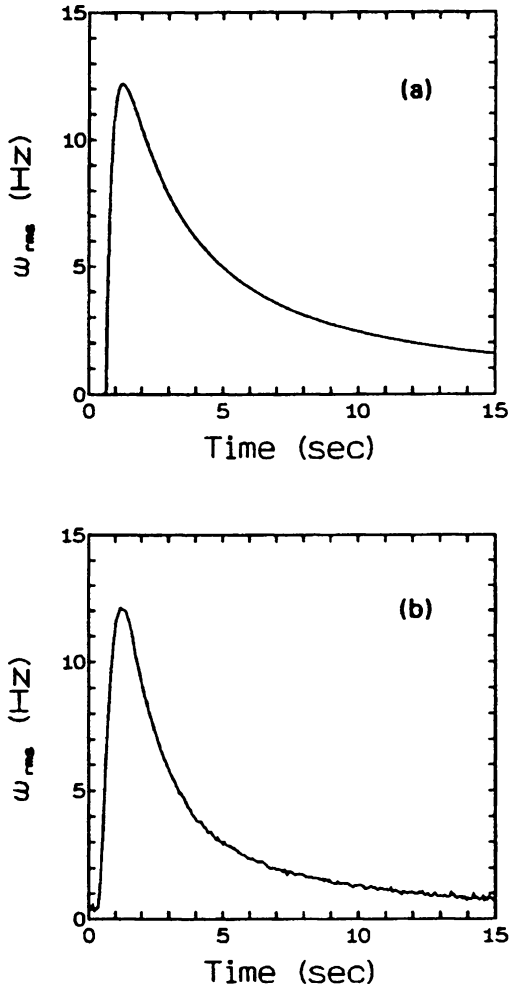

Figure 28. Theoretical (a) and observed (b) turbulent bursts. The theoretical curve is given by Chen and Goldenfeld (1992) and the experimental one is the result of many averages. In both cases $x = 1.137$ cm and $V = 50$ cm s^{-1} (Smith 1992).

It is not clear Q what should be for this experiment. The method of setting up the flow does not give any centre-of-mass motion to the fluid. The energy given to the fluid should just be the work done on the fluid, which is the force times the displacement of the grid. The simplest assumption is a linear relation which suggests Q should scale as the grid velocity V.

Barenblatt's analysis says the time t necessary for the peak of the burst to travel a particular distance h depends on Q as

$$t \sim Q^{-1/2}. \tag{4.69}$$

Results of arrival time as a function of grid towing velocity V are shown in figure 29. The exponent b used in the fit is obtained by calculating the variance in the fit as shown in figure 29(b) and has the value 0.5028 suggesting strongly that Q depends linearly upon V.

The dependence of h upon t is given by the data in figure 30. Here we have positioned the grid at different distances h from the detector and have observed the arrival of the peak.

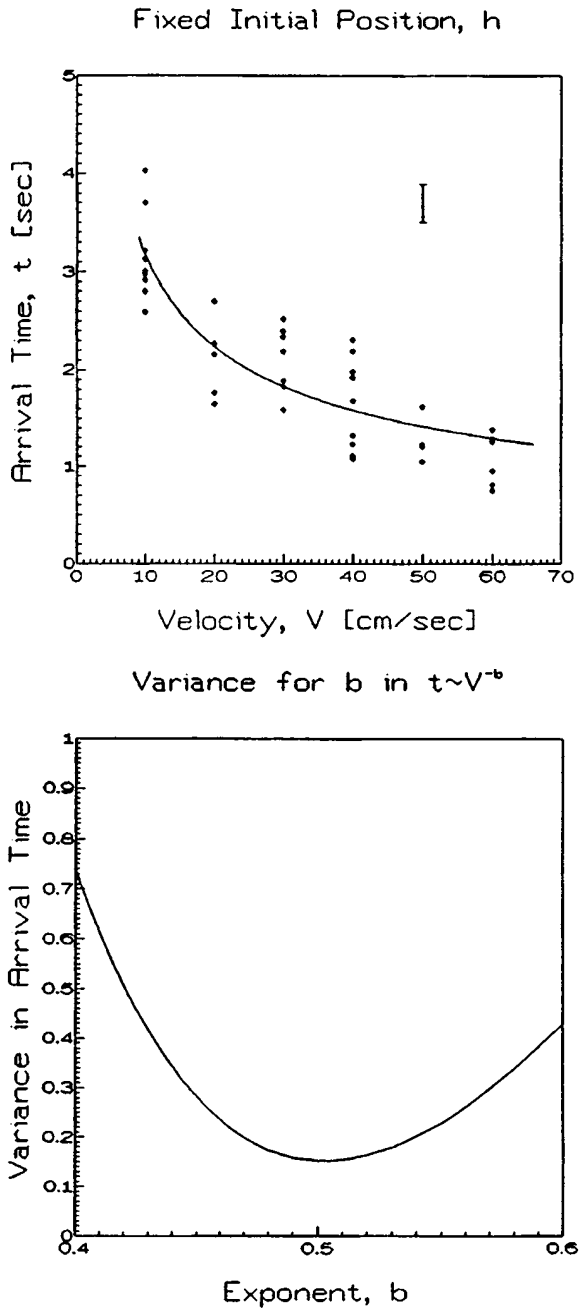

Figure 29. (a) Fit of arrival time as a function of towing velocity for a fixed initial position of 1 cm. The vertical bar is the standard deviation corresponding to the minimum variance in (b) (Smith 1992). (b) Variance in arrival time for the data in (a) as a function of the exponent b (Smith 1992).

A simple way to display this result is to plot $(3/2)\log h(t)$ against $\log t$. If Barenblatt is right, the data should have a slope of 1. The best fit of our data is shown in figure 31, and has a slope of ($\sim$1.028), showing impressive support for Barenblatt's prediction.

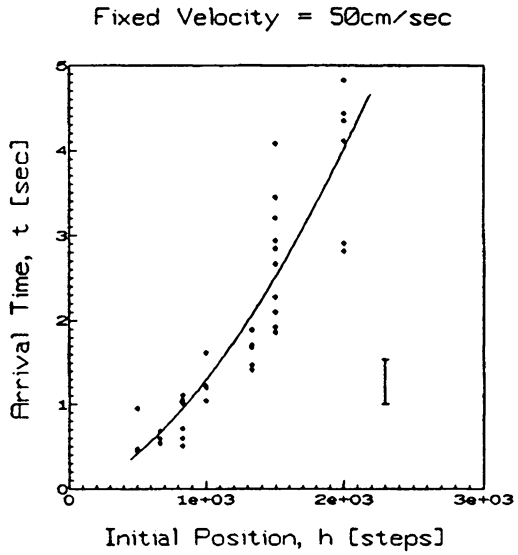

Figure 30. Fit of arrival time as a function of grid position for fixed towing velocity. The distance h is determined by a stepper motor, with 1000 steps approximately corresponding to 1 cm. The vertical bar is the standard deviation corresponding to the minimum variance in figure 29(b) (Smith 1992).

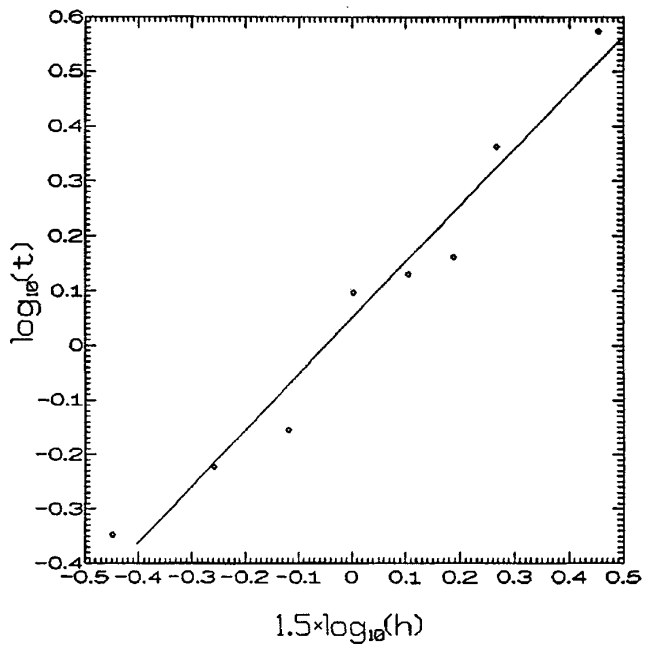

Figure 31. Plot of $(3/2)\log h(t)$ against t. The straight line is the best fit to Smith's data and has a slope of $\sim$1.028 (Smith 1992).

In a recent preprint Chen and Goldenfeld (1992) have re-examined Barenblatt's problem and have predicted that the dependence of h upon t is not quite $t^{2/3}$. Indeed they suggest that

$$h(t) \sim (Q^{1/2}t)^{(2/3)-\phi} \tag{4.70}$$

where ϕ is an 'anomalous dimension' depending on the dissipation. Smith (1992) made an attempt to determine ϕ from his data, but it is clear that this interesting result would benefit greatly from improvements to the sensitivity of our apparatus.

4.11. Turbulence at absolute zero

At temperatures low enough that the normal fluid fraction is negligible a convenient mathematical description of the superfluid is given by the nonlinear Schrödinger equation (NLSE), which describes a container of N bosons interacting via a delta function repulsive potential of strength V_c,

$$\mathrm{i}\hbar\frac{\partial\psi}{\partial t} = -\frac{\hbar^2}{2m}\nabla^2\psi - mE\psi + V_0\psi|\psi|^2 \tag{4.71}$$

where E is the energy per unit mass and the wavefunction ψ is normalized by $\int \mathrm{d}^3x\,|\psi|^2 = N$.

Equation (4.72) is not an exact description of superfluidity: it neglects the condensate's depletion and the existence of rotons in the dispersion relation. Nevertheless, it is a convenient tool since it captures some of the essential physics, for example it has vortex line solutions.

Writing ψ in terms of an amplitude and a phase

$$\psi = A\,\mathrm{e}^{\mathrm{i}F} \tag{4.72}$$

one has $\rho_s = mA^2$ and $v_s = (\hbar/m)\nabla F$. If we let $F = \varphi$ in cylindrical coordinates (r, φ, z) then we obtain Feynman's vortex line

$$v_s = \frac{\kappa}{2\pi r}\hat{\varphi} \tag{4.73}$$

where $\hat{\varphi}$ is the unit vector in the φ direction, together with a differential equation for ρ_s. The solution of this equation tends to the bulk density value $\rho_s \to m^2E/v_s$ for $r \to \infty$ and to zero on the vortex axis $\rho_s \to 0$ for $r \to 0$. The characteristic distance over which ρ_s changes is $\cong 10^{-8}$ cm, and is called the 'vortex core' parameter. We conclude that the vortex core is effectively hollow, that there is no singularity at $r \to 0$ (the velocity diverges but the density tends to zero so that the momentum is finite) and that $\nabla \times v_s = 0$ since v_s is the gradient of a phase, as envisaged by Landau.

The NLSE model has been used to demonstrate the existence of reconnections (Koplik 1993) which are postulated in the vortex dynamics approach of Schwarz. The NLSE has also been used to study turbulence tangles by Nore *et al* (1996). They made two major observations: the first is that the energy spectrum of the tangle has an inertial range compatible with the classical $-5/3$ law of Kolmogorov. The second is that as the tangle evolves, there is a significant transformation of kinematic energy into compressible sound energy. This second finding has lead Samuels and Barenghi (1998) to investigate the thermodynamic implications and to speculate that the production of sound is the fundamental process of dissipation of kinetic energy at $T = 0$.

On the experimental side, vortex tangles at very low temperatures are being studied at Lancaster University at temperatures around 70 mK.

A very recent approach, described in a recent preprint from Vinen (1999), is not based on the NLSE. It is based simply on the idea of vortex lines, which can reconnect, without looking at the detailed microscopic description of reconnection. It asks how energy can be lost from the tangle at $T = 0$ and at very low temperatures. It suggests that energy is fed into a cascade formed from Kelvin waves on the lines, with energy flowing into Kelvin waves of shorter and shorter wavelengths, like a kind of Kolmogorov cascade. Energy is ultimately lost from short-wavelength Kelvin waves, either by radiation of sound, at the very lowest temperatures, or

by frictional interaction with the residual normal fluid at slightly higher temperatures. Kelvin waves play a role only at very low temperatures: at higher temperatures the Kelvin waves of all relevant wavelengths are too strongly damped by mutual friction. These details lead to fairly clear predictions, which for the most part remain to be tested.

5. Conclusions, influence of Vinen on turbulence research

Looking back on research on turbulence since World War II, we can see more clearly than in times past the sweep of ideas and experiments. Immediately after the war there was a truly great era of turbulence research at Cambridge, building on the ideas and genius of G I Taylor, his associates G K Batchelor and A Townsend, and their research groups. There was also an appreciation of the enormous vigor and accomplishments of Soviet scientists such as Kapitza, Landau, Lifshitz, Khalatnikov, Ginzburg, Kolmogorov and others who considered fluid mechanics one of the greatest challenges in physics. Indeed, if I recall correctly, David Shoenberg was influential in getting early translation (by Michael Priestley) of Khalatnikov's important papers to the west. Henry and Joe made incredible progress in understanding the phenomenology of helium II (Vinen 1957a, b, c, 1958, Hall and Vinen 1956a, b, 1961a, b, Hall 1958).

The important thing to realize is that Vinen put his principal effort into a study of turbulence in helium II, at a time when turbulence was being completely neglected by physicists. Building on research at Leiden, supplemented by his own experiments and deep intuition, Vinen was able to give an account of the growth, equilibrium and decay of counterflow turbulence, which is still the generally accepted picture. And as I noted in section 4.2.1 it is clear that Joe and Henry were on their way to discovering quantized vortices experimentally when the theory of Onsager and Feynman first appeared.

Another remarkable achievement of Vinen was the introduction of the fluctuation theory of vortex nucleation (see Donnelly 1991b, ch 8). While this topic has not been part of the present discussion, it does not seem to be generally recognized that what is called the ILF (for Iordanskii, Langer and Fisher) theory of nucleation was actually first discussed by Vinen at the famous Enrico Fermi summer school held at Varenna in 1961 (Vinen 1961a).

Counterflow turbulence, the principle topic of the past half century, has really only three scales: the size of the apparatus, the intervortex spacing and the vortex core parameter. For that reason, among others, the understanding of this flow has proceeded relatively quickly. Fully aware of this fact, Vinen urged our laboratory to begin work on the towed grid apparatus, which generates a full spectrum of turbulent eddies and has been so productive for us over the years.

Never one to be idle, Joe has spent the past several years thinking about the decay of superfluid turbulence at and near absolute zero. The first fruits of this thinking are briefly described in section 4.11. As is usual when Vinen is around, my laboratory is buzzing with activity.

Acknowledgments

I am grateful to many people for help with this article, including C F Barenghi, M McAshan, J J Niemela, D C Samuels, L Skrbek, K R Sreenivasan and W F Vinen. The research of the author is supported by a grant DMR 9529609 from the National Science Foundation.

References

Aarts R G K M and DeWaele A T A M 1994 Numerical simulation of superfluid turbulence near the critical velocity 1994 *Physica* B **194–196** 725

Ahlers G 1969 Mutual friction in He II near the lambda transition *Phys. Rev. Lett.* **22** 54–6

Andronikashvili E L 1946 Direct observation of two types of motion in helium II *Z. Ekxp. Theor. Fiz* **16** 780–5

Arms R J and Hama F R 1965 Localized-induction concept on a curved vortex and motion of an elliptical vortex ring *Phys. Fluids* **8** 553–9

Atkins K R 1959 Third and fourth sound in liquid helium II *Phys. Rev.* **113** 962–5

Awschalom D D, Milliken F P and Schwarz K W 1984 Properties of superfluid turbulence in a large channel *Phys. Rev. Lett.* **53** 1372–5

Baehr M L and Tough J T 1985 Dissipation in combined normal and superfluid flows of He II: a unified description *Phys. Rev.* B **32** 5632–8

Barenblatt G I 1983 *Nonlinear Dynamics and Turbulence*

Barenghi C F 1982 Experiments on quantum turbulence *Thesis* Physics, University of Oregon, Eugene

——1992 Vortices and the Couette flow of helium II *Phys. Rev.* B **45** 2290

Barenghi C F, Donnelly R J and Vinen W F 1983a Friction on quantized vortices in helium II. A review *J. Low Temp. Phys.* **52** 189–247

Barenghi C F, Hills R N and Donnelly R J 1983b Cubic spline fit to the 1958 4He scale of temperatures *J. Low Temp. Phys.* **51** 319–27

Barenghi C F and Jones C A 1987 On the stability of superfluid helium between rotating concentric cylinders *Phys. Lett.* A **122** 425

——1988 The stability of the Couette flow of helium II *J. Fluid Mech.* **197** 551

Barenghi C F and Samuels D C 1999 Self-consistent decay of superfluid turbulence *Phys. Rev.* B

Barenghi C F, Samuels D C, Bauer G H and Donnelly R J 1997 Superfluid vortex lines in a model of turbulent flow *Phys. Fluids* **9** 2631–43

Barenghi C F, Swanson C E and Donnelly R J 1982 Induced vorticity fluctuations in counterflowing He II *Phys. Rev. Lett.* **48** 1187–9

——1983c Rotation of a tangle of quantized vortex lines in He II *Phys. Rev. Lett.* **50** 190–3

——1995a Emerging issues in helium turbulence *J. Low Temp. Phys.* **100** 385–413

——1995b Quantized vortices between counterrotating cylinders *J. Low Temp. Phys.* **99** 143–50

Batchelor G K 1953 *The Theory of Homogeneous Turbulence* (Cambridge: Cambridge University Press)

Behringer R P 1990 Critical Rayleigh numbers for cryogenic experiments *J. Low Temp. Phys.* **78** 231–46

Benson C B and Hollis Hallett A C 1956 The oscillating sphere at large amplitudes in liquid helium *Can. J. Phys.* **34** 668–78

Bielert F and Stamm G 1993 Visualization of Taylor–Couette flow in superfluid helium *Cryogenics* **33** 938

——1994 Influence of quantized vortex lines on the stability of Taylor–Couette flow in helium II *Physica* B **194** 561

Bon Mardion C, Claudet G and Seyfert P 1978 Steady state heat transport in superfluid helium at 1 bar *Proc. 7th Int. Cryogenic Conf. (1978)* pp 214–21

Chen L-Y and Goldenfeld N 1992 *Phys. Rev.* A **45** 5572–7

Cheng D, Cromar M W and Donnelly R J 1973 Influence of an axial heat current on negative ion trapping in rotating helium II *Phys. Rev. Lett.* **31** 433–6

Chrandrasekhar S and Donnelly R J 1957 The hydrodynamic stability of helium II between rotating cylinders *Proc. R. Soc.* **A241** 9–28

Dickinson S C and Long R R 1978 Laboratory group of the growth of a turbulent layer of fluid *Phys. Fluids* **21** 1698–701

Dombre T, Greene J M, Henon H, Mehr A and Sowards A M 1986 Chaotic streamlines in the ABC flows *J. Fluid Mech.* **167** 353

Donnelly R J 1959 Experiments on the hydrodynamic stability of helium between rotating cylinders *Phys. Rev. Lett.* **3** 507–8

——1967 Experimental superfluidity *Chicago Lectures in Physics* ed W I Glaberson and P E Parks (Chicago, IL: University of Chicago Press)

——1989 Externally modulated hydrodynamic systems *NATO Workshop (Streitberg, Bayreuth, 1989)* (New York: Plenum)

——1991a Liquid and gaseous helium as test fluids *High Reynolds Number Flows Using Liquid and Gaseous Helium* ed R J Donnelly (Berlin: Springer)

——1991b *Quantized Vortices in Helium II* (Cambridge: Cambridge University Press)

Donnelly R J 1998 Flow at ultra-high Reynolds and Rayleigh numbers *A Status Report Including Papers from the Int. Workshop on Ultra-High Reynolds Number Flows Using Cryogenic Helium (Brookhaven National Laboratory, June 18–20, 1996)* ed R J Donnelly and K R Sreenivasan (New York: Springer)

Donnelly R J, Barenghi C F and Swanson C 1981 Measurements of vortex line density in counterflowing He II *Physica* **108B** 1131–2

Donnelly R J and Fetter A L 1966 Stability of superfluid flow in an annulus *Phys. Rev. Lett.* **17** 747–50

Donnelly R J and Hollis Hallett A C 1958 Periodic boundary layer experiments in liquid helium *Annals Phys.* **3** 320–45

Donnelly R J and LaMar M M 1988 Flow and stability of helium II between concentric cylinders *J. Fluid Mech.* **186** 163–98

Donnelly R J and Penrose O 1956 Oscillations of liquid helium in a U-tube *Phys. Rev.* **103** 1137–44

Dowley M W, Firth D R and Hollis Hallett A C 1961 *Proc. 7th Int. Conf. on Low Temperature Physics*

Feynman R P 1955 Application of quantum mechanics to liquid helium *Progress in Low Temperature Physics* ed C J Gorter (Amsterdam: North-Holland)

Galloway D J and Proctor M R E 1992 Numerical calculations of fast dynamos in smooth velocity fields with realistic diffusion *Nature* **256** 691

Gilbert A D, Otani N F, and Childress S 1993 Simple dynamical fast dynamos *Solar and Planetary Dynamos* ed M R E Proctor, P C Matthews and A M Rucklidge (Cambridge: Cambridge University Press)

Gorter C J 1949 On the irreversible processes in liquid helium II *Physica* **15** 285–304

Hall H E 1958 An experimental and theoretical study of torsional oscillations in uniformly rotating liquid helium II *Proc. R. Soc.* A **245** 546–61

——1960 The rotation of helium II 1960 *Phil. Mag. Suppl.* **9** 89–146

Hall H E and Vinen W F 1956a The rotation of liquid helium II. I. Experiments on the propagation of second sound in uniformly rotating helium II *Proc. R. Soc.* A **238** 204–14

——1956b The rotation of liquid helium II. II. The theory of mutual friction in uniformly rotating helium II *Proc. R. Soc.* A **238** 215–34

Hall S, Honey R and Donnelly R J 1999 Experiments on turbulence generated by an oscillating grid *Preprint*

Heikkila W and Hollis Hallet A C 1955 The viscosity of liquid helium II *Can. J. Phys.* **33** 420–35

Henderson K L and Barenghi C F 1994 Vortex tension and the stability of Couette flow in helium II *Physica* B **194–196** 567

——1999 The anomalous motion of superfluid helium in a rotating cavity *J. Fluid Mech.*

Henderson K L, Barenghi C F and Jones C A 1995 Nonlinear Taylor-Couette flow of helium II *J. Fluid Mech.* **281** 329

Hills R N and Roberts P H 1977 Superfluid mechanics for a high density of vortex lines *Arch. Rat. Mech. Anal.* **66** 43

Hollis Hallet C 1955 Oscillating disks and rotating cylinder in liquid helium II *Progress in Low Temperature Physics* ed C J Gorter (Amsterdam: North-Holland)

Jones C A, Khan K, Barenghi C F and Henderson K L 1995 The appearance of vortices in helium II *Phys. Rev.* B **51** 16 714

Jones C A, Putterman S J and Roberts P H 1986 A Bose condensate V. Stability of solitary wave solutions of the non-linear Schrodinger equation in two and three dimensions *J. Phys. A: Math. Gen.* **19** 2991–3011

Jones C A and Roberts P H 1982 Motions in a Bose condensate IV. Axisymmetric solitary waves *J. Phys. A: Math. Gen.* **15** 2599–619

Keesom H W, Keesom A P and Saris B F 1938 A few measurements on the heat conductivity of liquid helium II *Physica* **5** 281–5

Keesom W H and Keesom A P 1936 On the heat conductivity of liquid helium *Physica* **3** 359–60

Khalatnikov I M 1963 *An Introduction to the Theory of Superfluidity* (New York: Benjamin)

Koplik J 1993 Vortex reconnection in superfluid helium *Phys. Rev. Lett.* **71** 1375–8

Laing R A and Rorschach H E 1961 Hydrodynamic drag on spheres moving in liquid helium *Phys. Fluids* **4** 564–71

Landau L D 1941 The theory of superfluidity of helium II 1941 *J. Physique (Moscow)* **5** 71–114

Landau L D and Lifshitz E M 1969 *Statistical Physics (Course of Theoretical Physics vol 5)* 2nd edn (London: Pergamon)

Lorenson C P, Griswold D, Nayak V U and Tough J T 1985 Dynamic features of superfluid turbulence near the second critical heat current *Phys. Rev. Lett.* **55** 1494–7

Martin K P and Tough J T 1983 Evolution of superfluid turbulence in thermal counterflow *Phys. Rev.* B **27** 2788–99

Matheiu P, Serra A and Simon Y 1976 Critical-region measurements of the mutual friction parameters in rotating helium II *Phys. Rev.* B **14** 3755–61

Melotte D J and Barenghi C F 1998 *Phys. Rev. Lett.* **80** 4181

Moffat H K and Tsinobar A 1992 Helicity in laminar and turbulent flows *Ann. Rev. Fluid Mech.* **24** 281

Niemela J J and Donnelly R J 1991 Thermal convection in liquid helium *Proc. Conf. on High Reynolds Number Flows Using Liquid and Gaseous Helium (New York, 1991)*

Nore C, Abid M and Brachet M E 1996 Kolmogorov turbulence in low-temperature superflows *Phys. Rev. Lett.* **78** 3896–9

Onsager L 1949 Discussion on a paper by C J Gorter *Nuovo Cimento Suppl.* **6** 249–50

Opatowsky L B and Tough J T 1981 Homogeneity of turbulence in pure superflow *Phys. Rev.* B **24** 5420–1

Osborne D V 1950 The rotation of liquid helium 1950 *Proc. Phys. Soc.* A **63** 909–12

Ostermeier R M and Glaberson W I 1975 Instability of vortex lines in the presence of axial normal fluid flow *J. Low Temp. Phys.* **21** 196

Otto S R 1992 On stability of the flow around an oscillating sphere *J. Fluid Mech.* **239** 47–63

Roberts P H and Donnelly R J 1974 Superfluid mechanics *Annual Review of Fluid Mechanics* (Palo Alto: Annual Reviews Inc)

Samuels D C 1992 Velocity matching and Poiseuille pipe flow of superfluid helium *Phys. Rev.* B **46** 11 714–24

Samuels D C and Barenghi C F 1998 Vortex heating in superfluid helium at low temperature *Phys. Rev. Lett.* **81** 4381–3

Samuels D C and Donnelly R J 1990 Dynamics of the interactions of rotons with quantized vortices in helium II *Phys. Rev. Lett.* **65** 187–90

Schlichting H 1979 *Boundary-Layer Theory* 7th edn (New York: McGraw-Hill)

Schwarz K W 1979 Turbulence in superfluid helium: steady homogeneous counterflow *Phys. Rev.* B **18** 245–62

——1982 Generating superfluid turbulence from simple dynamical rules *Phys. Rev. Lett.* **49** 283–5

——1983 Critical velocity for a self-sustaining vortex tangle in superfluid helium *Phys. Rev. Lett.* **50** 364–7

——1985 Three-dimensional vortex dynamics in superfluid ^{4}He: line–line and line–boundary interactions *Phys. Rev.* B **31** 5782–804

——1998 Three-dimensional vortex dynamics in superfluid 4 Helium: homogeneous superfluid turbulence *Phys. Rev.* B **38** 2398–417

Schwarz K W and Rozen J R 1991 Anomalous decay of turbulence in superfluid ^{4}He *Phys. Rev. Lett.* **66** 1868

She Z S, Jackson E and Orszag S A 1990 Intermittent vortex structures in homogeneous isotropic turbulence *Nature* **344** 226

Smith M R 1992 Evolution and propogation of turbulence in helium II *PhD Thesis* University of Oregon

Smith M R, Donnelly R J, Goldenfeld N and Vinen W F 1993 Decay of vorticity in homogeneous turbulence *Phys. Rev. Lett.* **71** 2583–6

Smith M R, Hilton D K and Van Sciver S W 1999 Observed drag crisis on a sphere in flowing He I and He II *Phys. Fluids.* **11** 751–3

Snyder H A 1974 Rotating Couette flow of superfluid helium *Proc. 13th Int. Conf. on Low Temperature Physics-LT13 (1974)* (New York: Plenum) vol 1 pp 283–7

Stalp S 1998 Decay of grid turbulence in superfluid helium *PhD Dissertation* Physics, University of Oregon, Eugene

Stalp S, Skrbek L and Donnelly R 1999 Decay of grid turbulence in a finite channel *Phys. Rev. Lett.* **82** 4831–4

Swanson C E and Donnelly R J 1985 Vortex dynamics and scaling in turbulent counterflowing helium II *J. Low Temp. Phys.* **61** 363–9

——1987 The appearance of vortices in the flow of helium II between rotating cylinders *J. Low Temp. Phys.* **67** 185–93

——1991 Instability of Taylor–Couette flow of helium II *Phys. Rev. Lett.* **67** 1578–81

Tisza L 1938 Transport phenomena in helium II *Nature* **141** 913

Tough J T 1982 Superfluid turbulence *Progress in Low Temperature Physics* ed D F Brewer (Amsterdam: North-Holland)

Vinen W F 1957a Mutual friction in a heat current in liquid helium II, I. Experiments on steady heat currents *Proc. R. Soc.* **A240** 114–27

——1957b Mutual friction in a heat current in liquid helium II, II. Experiments on transient effects *Proc. R. Soc.* **A240** 128–43

——1957c Mutual friction in a heat current in liquid helium II, III. Theory of the mutual friction *Proc. R. Soc.* **A242** 493–515

——1958 Mutual friction in a heat current in liquid helium II, IV. Critical heat currents in wide channels *Proc. R. Soc.* **A243** 400–13

——1961a Critical velocities in liquid helium II *Int. School of Physics 'Enrico Fermi'*

——1961b Vortex lines in liquid helium II *Progress in Low Temperature Physics* ed C J Gorter (Amsterdam: North-Holland)

——1999 Why is turbulence in a quantum fluid often similar to that in a classical fluid? *Phys. Rev.* submitted

von Neumann J 1949 Recent theories of turbulence *Collected Works* ed A H Taub (Oxford: Pergamon)

Walstrom P L, Weisend II J G, Maddocks J R and Van Sciver S W 1988 Turbulent flow pressure drop in various helium II transfer system components *Cryogenics* **28** 101–10

Wang R T, Swanson C E and Donnelly R J 1987 Anistropy and drift of a vortex tangle *Phys. Rev.* B **36** 5240–4
Wheeler R G, Blackewood C H and Lane C T 1955a Second sound attenuation in rotating helium II *Phys. Rev.* 1667–72
——1955b Second sound attenuation in rotating helium II *Phys. Rev.* 1196
Wilks J 1967 *The Properties of Liquid and Solid Helium (International Series of Monographs on Physics)* ed W Marshall and D H Wilkinson (Oxford: Clarendon)
Wolf P E, B P, Hulin J P and Elleaume P 1981 Rotating Couette flow of helium II *J. Low Temp. Phys.* **36** 381–430
You Y B 1993 Remnant vortices of helium II between rotating concentric cylinders *PhD Thesis* University of Oregon